INTERNATIONAL JOURNAL OF
IJCOE
COASTAL, OFFSHORE & ENVIRONMENTAL ENGINEERING

Volume 1 | Issue 1 | Apr 2016

www.ijcoe.org

info@ijcoe.org

Volume 1 | Issue 1| Apr 2016

International Journal of Coastal, Offshore and Environmental Engineering (IJCOE) | Vol. 1 / Issue. 1 / Apr 2016

International Journal of
Coastal, Offshore & Environmental Engineering
Since 2015
ISSN: 2980-8731 (online)

IJCOE
Editor-in-Chief: Prof. Hamid S.Bahai

International Journal of Coastal, Offshore & Environmental Engineering
Since 2015
ISSN: 2980-8721 (online)

In The Name of God

Message from the Editor-in-Chief

The IJCOE journal office was established in 2015,and its first issue was published in 2016. TheIJCOE covers a wide range of research in thefields of oceanography & ocean technology, aswell as marine industries & marine engineering.The editorial board of IJCOE consists of nearly130 of the greatest scientists and researchersfrom over 30 countries worldwide, and thejournal's review board comprises 1,000 membersfrom all five continents. The membership andapplication process for joining the editorial andreview boards of this journal is ongoing. IJCOE isa research-academic quarterly journal that haspublication and distribution permissions fromthe Press Organization and permission topublish scientific-research articles from theMinistry of Science, Research, and Technology(MSRT) with an "A" rating. It also holds a "Q1"rating from the ISC institute with an impactfactor (IF) of approximately 0.43 and isconsidered a "core journal" (prestigious andoutstanding journal). IJCOE is an open-accessjournal and allows the download and receipt ofaccepted articles in full text for free. It respectsand adheres to copyright and COPE regulations.The journal's office operates 24/7, providingservices to researchers. In addition to publishinga regular quarterly journal, IJCOE has 16 specialissues on specific topics in preparation. It alsoprovides conditions for publishing specializedbooks, references, and handbooks. Moreover, itis ready to cooperate with the secretariats ofreputable international conferences to publishtheir selected and outstanding articles. IJCOEevaluates, appraises, and publishes books,articles, and the scientific achievements andfindings of esteemed researchers and scientistsworldwide who are innovating and conductingin-depth research in the "important and strategicfield of the maritime technology & Oceanengineering." It welcomes any form of jointcooperation with universities, research institutes,and related research centers at the national,regional, and international levels, and extends ahand for collaboration.

Classification of Editorial Board in IJCOE

- Editor-in-Chief
- Director-in-Chief
- Deputy Editor
- Executive Managers
- English Text Editor
- Technical Editor
- International Editorial Board
- National Editorial Board
- Editorial Board Associate
- Editorial Board Assistant
- Guest Editorial Board
- Advisory Board
- Administrative Coordinator
- Honorary Board Member
- Methodology Advisor

Author Benefits

- Open Access
- Rapid Publication
- Thorough Peer-Review
- No Copyright Constraints
- Coverage by Leading Indexing Services
- Discounts On Article Processing Charges (APC)
- No Space Constraints, No restriction on the maximum length of the papers, number of figures or colors

INTERNATIONAL JOURNAL OF IJCOE COASTAL, OFFSHORE & ENVIRONMENTAL ENGINEERING

Aims of IJCOE

Hydrodynamics

Marine equipment

Structural mechanics

Ocean environmental predictions

Stochastic calculations Experimental

Automatic Control of Marine Systems

Scope of IJCOE

Marine Hazards

Ocean Acoustics

Naval Architecture

Ocean Engineering

Coastal Engineering

Marine Meteorology

Marine Earth Sciences

Underwater Technology

Marine Renewable Energy

Polar & Arctic Engineering

Marine Renewable Energy

Marine Geography & Geodesy

Marine Environmental Engineering

Automatic Control of Marine Systems

Hydro Physics & Physical Oceanography

Type of papers

- Case Studies
- Book Reviews
- Review Article
- Letters to the Editor
- Methodology Papers
- Editorials and Commentaries
- Response or Rejoinder Papers
- Perspective or Opinion Papers
- Conceptual or Theoretical Papers
- Meta-Analysis and Systematic Reviews
- Short Communications or Brief Reports
- Research Articles (Original Research Papers)

Scientific Research Journal

Ministry of Science, Research And Technology (MSRT)

Jurnal Ranking 2023: A

Ministry Of Science, Research And Technology (ISC)

Citation Impact 2022: 0.429

Quartile 2022 : Q1

Core Collection

IJCOE is a Member of

Cantact Us

Office 1 | Research Institute of Meteorology and Atmospheric Science

Address | Tehran, Shahid Kharrazi Highway, Pajoohesh Blvd, Research Institute of Meteorology and Atmospheric Science, Sand and Dust Storm International Research Center (SDS-IRC), No. 13, 1st floor.

Phone | +982144787652

Postal code | 13611-14977

website | www.rimac.ac.ir

Office 2 | Iranian National Institute for Oceanography and Atmospheric Science

Address | Tehran, Dr. Fatemi Gharbi St., Shahid Etemadzade St., No. 3, third floor.

Phone | +982166944873

Postal code | 13389 – 14118

website | www.inio.ac.ir

Email | Info@ijcoe.org

Website | www.ijcoe.org

Follow Us

www.ijcoe.org

INTERNATIONAL JOURNAL OF IJCOE COASTAL, OFFSHORE & ENVIRONMENTAL ENGINEERING

Volume & Issue:

Volume 1, Issue 1, April 2016

Number of Articles: 5

Content

INTERNATIONAL JOURNAL OF
COASTAL & OFFSHORE ENGINEERING
JCOE No. 1/ Winter 2016 (1-6)

Stress Concentration Factors in FRP Strengthened Tubular T-joints Under Brace In-Plane Bending and Out-of-Plane Bending Moments

Alireza Sadat Hosseini[1]*, Mohammad Reza Bahaari[2], Mohammad Lesani[3]

[1]*PhD Candidate, University of Tehran; a.sadat@ut.ac.ir*
[2]*Assocciate Professor, University of Tehran; mbahari@ut.ac.ir*
[3]*Assisstant Professor, University of Tehran; m.lesani@sadra.ac.ir*

ARTICLE INFO

Article History:
Received: 22 Sep. 2016
Accepted: 15 Mar. 2016

Keywords:
Tubular T-joint
FRP
SCF
IPB
OPB
Finite Element

ABSTRACT

This research is dedicated to study the relative stress concentration factors (SCF) at FRP strengthened tubular T-joint subjected to brace in-plane and out-of-plane bending moments using Finite Element Analyses performed by ABAQUS software package. Validation analysis for the finite element model of the unstiffened joint is performed against the experimental results together with the Lloyd's Register and API equations. The effectiveness of using three different types of FRP materials such as Glass/Vinyl ester, Glass/Epoxy (Scotch ply 1002) and Carbon/Epoxy (T300-5208) on enhancing the fatigue life of tubular T-joints through computing the SCFs was investigated in three schemes. At first the chord alone was strengthened in order to investigate the effects of strengthening the chord member on SCFs. In the second phase, FRP was applied only on the brace member to study the brace strengthening effects, and in the third phase, both of the chord and brace members were strengthened. Promising results derived from analysis which show that FRP strengthening method can effectively decrease the SCF values at T-joints.

1. Introduction

In offshore steel jackets circular hollow sections (CHS) are the load bearing members. CHSs are chosen due to their adequate structural performance against bending, buckling and torsion and also another advantages such as high strength-to-weight ratio, high buoyancy and lower drag coefficients [1]. T-joints are the most common and basic CHS joint configuration which are made by welding the cross section of one tube (brace) perpendicular to the undisturbed exterior surface of the other tube (chord).

Offshore steel jackets are subjected to repeated loading and unloading cycles due to the cyclic nature of wave loading. Therefore, care must be given to fatigue phenomenon in such structures. Thus, in order to ensure structural safety, prediction of fatigue life of offshore structural joints and accurate estimation of fatigue load resistance are necessary. Fatigue life of offshore structures is normally assessed using Stress-Life (S-N) curves. In this way, hot-spot stress range (HSSR) is calculated from a parameter called the stress concentration factor (SCF). According to API-Part 8.3.1 [2], "For each tubular joint configuration and each type of brace loading, SCF is defined as: The hot spot stress range (HSSR)/nominal brace stress range". Here in this research we concentrated on estimation of SCFs at chord member. So, the HSSR is the hot spot stress range on the chord which must be divided by the nominal direct stress in the brace member to give the SCF. Having HSSR, and using S-N curves, the number of loading cycles that the structure can sustain before failure could be estimated. SCFs can be considered in unstiffened and stiffened joints. In unstiffened joints, many researchers did efforts since the 1970s and their main objective was to derive parametric equations for the SCF calculation. Lesani et al. [3] reviewed some of the strengthening techniques of CHSs. There are metallic as well as non-metallic external reinforcement schemes such as FRP strengthening technique. FRP wrapping method due to its convenience for handling and application, potentially high overall durability, corrosion resistance, light weight, superior strength-to-weight ratio, tailorability and high specific performance attributes with respect to steel, could be easier for application in areas which conventional materials may encounter durability, weight or lack of design flexibility constraints. As examples of studies on FRP strengthened steel structures, researches done by Hollaway and Cadei [4], Zhao and Zhang [5] and Zhao [6] are remarkable. FRP-strengthened CHSs with four layers of CFRP under tension loading was

investigated by Jiao and Zhao [7]. Zhao et al. [8] studied the load bearing capacity of RHSs strengthened with CFRP sheets. Lesani et al. [3] numerically investigated the failure pattern, ultimate static strength and detailed behavior of steel tubular T-joints strengthened by GFRP (Glass/epoxy) under axial brace compressive loading. Remarkable increase in joint ultimate capacity due to the combined action of steel and composite against the compressive load was observed. In addition, critical deformations and ovalization of chord member showed a descending trend up to 50% of the un-strengthened joint. Lesani et al. [9] experimentally investigated the improvement of ultimate capacity of T-joints wrapped with GFRP (Glass/vinyl ester) under static compressive loading. Increase up to 50% in the ultimate load bearing capacity of the tubular joint strengthened by FRP was observed. A numerical and experimental research program was conducted by Lesani et al. [10] on T and Y shaped CHS steel tubular connections strengthened with GFRP. This research showed numerically and experimentally that, the static strength of tubular joints could be improved significantly by the FRP wrapping technique. Based on the improvements observed in the static strength, investigation of SCF improvement and fatigue strength enhancement using the FRP wrapping technique seems to be necessary. The present research is aimed on such investigations on relative SCF values not addressed in previously studies. In this paper, the results of numerical analyses on FRP-strengthened steel tubular T-joints were used to present the effect of FRP material type on the SCF distribution along the weld toe under brace axial loading, and also the SCF values at crown and saddle positions under in-plane and out-of-plane bending moments respectively using Finite Element Analyses performed by ABAQUS software package. The finite element models of the unstiffened joints were verified against the experimental results extracted from HSE OTH 354 report [11] and the predictions of Lloyd's Register (LR) [11] and API [2] equations. The results of analysis on stiffened finite element models could address how FRP properties can affect the SCF values and accordingly the fatigue life the strengthened T-joint under three major types of loadings.

Finite Element Modeling and Verification

Here, finite element models were developed and analysis were carried out using ABAQUS software package [12]. The T-joints were chosen from JISSP project experimental results [11], JISSP joint 1.13. Three types of common FRP materials, Glass/vinyl ester, Glass/epoxy (Scotch ply 1002) and Carbon/epoxy (T300-5208), are used as strengthening material on the T-joints in order to find out how FRP wrapping affects the SCF values through the parametric study. Table 1 demonstrates the properties of the FRP materials used in the analyses. In this table, subscripts ''1'' and ''2'' stand for the fiber longitudinal and transverse directions respectively.

In order to achieve accurate stresses along the chord-brace intersection, the weld profile should be modeled accurately. Here, the weld profile along the brace-chord intersection satisfies the specifications addressed in AWS [14]. In Figure 1b the weld profile section in finite element model can be seen. In this study, ABAQUS 3D brick elements are incorporated to model the joint geometry and weld profile after the sensitivity analysis. Element type C3D20 which is a 20-node quadratic brick is used to model the joint. FRP material is modeled using shell elements defined as a skin layer on the joint. ABAQUS element type S4R, which is a 4-node doubly curved thin or thick shell with reduced integration is used to model the FRP skin layers. FRP mesh elements are tied to the solid elements of the un-stiffened joint geometry, in other words, a perfect bond state was considered and no cohesive/adhesive element was modeled at the FRP and the steel substrate interface. This is not a irrational assumption since the bound between FRP layer and steel stays undisturbed in the elastic range of loading according to the experimental and numerical analysis by Lesani et al. [9].

Different sub-zone mesh generation methods was used for the weld profile, hot spot stress region, FRP wrapping area and other regions of the joint. The mesh in the hot-spot stress region is much finer than the other zones since more computational precision is required in this area. FRP wrapping areas have coarser meshes but still fine enough to ensure computational accuracy. Figure 1 shows the mesh generated for the tubular T-joint.

Table 1: FRP properties [13]

	E_1 (Mpa)	E_2 (MPa)	ν_{12}	G_{12} (MPa)	G_{13} (MPa)	G_{23} (MPa)
Glass/ Vinyl ester	28000	7000	0.29	4500	4500	2540
Glass/Epoxy (Scotch ply 1002)	38600	8270	0.26	4140	4140	3100
Carbon/Epoxy (T300-5208)	132000	10800	0.24	5700	5700	3400

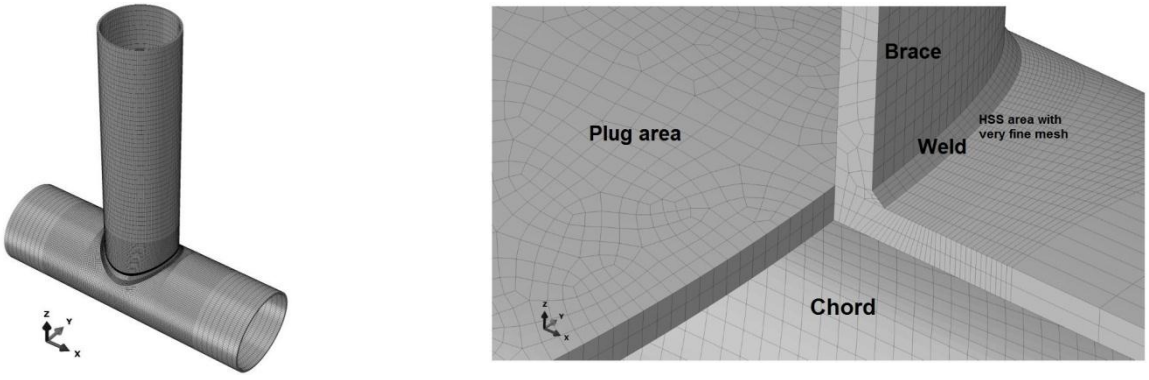

(a) (b)

Figure 1: The mesh generated for the T-joint (JISSP joint 1.13) using the sub-zone method: a) Isometric view; b) Mesh enlargement

As previously mentioned, the tubular T-joints in this study are modeled based on the joint properties given in JISSP project [11]. Thus, all the brace and chord geometry details are modeled according to JISSP joint 1.13 [11].

The boundary conditions are chosen in such a way to represent the actual boundary conditions of the experiment. Here in the analyses, chord ends were assumed to be fixed.

In order to determine the stress concentration factors in a tubular joint, a linear elastic numerical analysis needs to be performed [15]. The Young's modulus and Poisson's ratio of steel are taken as 207 GPa and 0.3, respectively. In order to estimate the SCFs, the method introduced by IIW-XV-E [16] is implemented. In this method, the peak stress at the weld toe is calculated by linear extrapolating the von-Mises stresses at distances of 0.4T and 1.4T from the weld toe; where T is the thickness of the chord member. SCF is calculated by dividing the von Misses stresses at weld toe by the nominal stress in the brace. In order to validate the finite element model, Lloyd's Register equations [11] and API [2] equations for SCF computation together with the test results published in HSE OTH 354 report for JISSP joint 1.13 were used. Table 2 summarizes the verification results at the saddle and crown points. In this table, e_1 and e_2 show the percentage of relative difference of Lloyd's Register [11] and API [2] equations with test results respectively, and e_3 denotes the percentage of relative difference between the results of finite element model and the experiment results. According to Table 2, it is obvious that the finite element model predicts the SCFs at crown and saddle points accurately which is in good agreement with the test results and therefore, the FE model is validated.

Where D is the chord diameter; α=2L/D, L is the chord length; β=d/D, d is the brace diameter; γ=D/2T, T is the chord thickness; τ=t/T, t is the brace thickness.

Analysis and Results

Here the analyses and results on the strengthened joints are explained. In order to investigate the stress concentration in FRP strengthened tubular T-joints under brace in-plane and out-of-plane bending moments, models were generated and analyzed using ABAQUS finite element software package. Stresses along the chord-brace intersection and correspondingly the SCF values could strongly be affected by change in FRP mechanical properties due to change in fiber and/or matrix material. The three mentioned FRP materials (Glass-vinyl ester, Glass-epoxy and Carbon-epoxy) were used for strengthening. Analyses were carried out in three phases. At first, the chord alone was strengthened in order to investigate the effects of strengthening the chord member on SCFs (Figure 2a). In the second phase, FRP was applied only on the brace member to study the brace strengthening effects (Figure 2b), and finally in the third phase, both of the chord and brace members were strengthened (Figure 2c). SCFs are calculated in Crown and Saddle points. Details and results of the analyses on SCF values in strengthened T-joints are as follow.

Table 2: Comparison of finite element results with experimental data [11] and predictions of Lloyd's Register (LR) [11] and API [2] equations

Reference	D (mm)	α	β	γ	τ	Load / Position	Test	LR Eq.	API Eq.	FEM	e_1 (%)	e_2 (%)	e_3 (%)
JISSP joint 1.13	508	6.2	0.8	20.3	1.07	IPB / Crown	3.9	4.07	4.85	3.92	4.4	24.4	0.5
						OPB / Saddle	12.2	18.2	15.3	10.1	49.2	25.4	-17.2

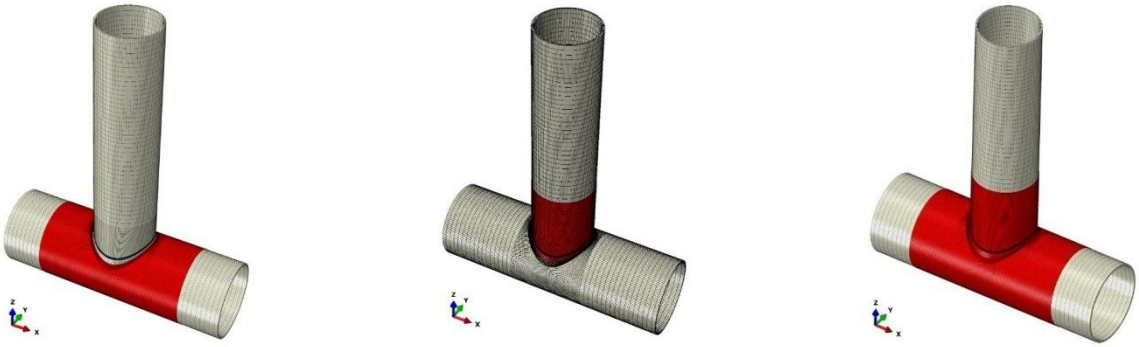

(a) (b) (c)

Figure 2: A typical FRP wrapped T-joint: a: Chord strengthening; b) Brace strengthening; c) Chord and brace strengthening

SCF values at crown and saddle points of the strengthened T-joint (JISSP joint 1.13) were investigated subject to IPB and OPB loadings. In all models, the applied FRP has a thickness of 1 mm, wrapping length equal to the diameter of the relative strengthened member (1D for chord member and 1d for brace member, where D and d are the chord and brace diameters respectively).

FRP materials were applied on the joint fibers in both 0° and 90° orientations. The effects of FRP material when the chord member, the brace member, and both chord and brace members were strengthened are presented in Figure 3 and 4 for IPB and OPB loadings respectively. In these figures, for instance, Ch0 stands for the strengthened chord which has 0° fiber orientation and Br90 is the strengthened brace with 90° fibers orientation. When both chord and brace members were strengthened, for instance, "Ch0Br90" is a synthetic strengthened joint (Both chord and brace members were stiffened) with 0° fibers orientation at chord and 90° fibers orientation at brace. In other words, the chord and brace FRP fibers are along the transverse (hoop) direction. According to Figure 3, in case of IPB loading, when only the chord member was strengthened with 90° fibers, the SCF values were reduced effectively, while for OPB loading, according to Figure 4, the most decreasing effect on SCFs was observed when fibers were placed in 0° orientation in the strengthened chord. Brace strengthening had an adverse effect on SCF values. Besides, change in material properties shows more considerable alteration on SCF values when FRP fibers are in 90° and 0° in IPB and OPB loadings respectively. Focusing on these figures reveals that the strengthened brace with 0° fibers has the highest decreasing effect on the SCF amplitude.

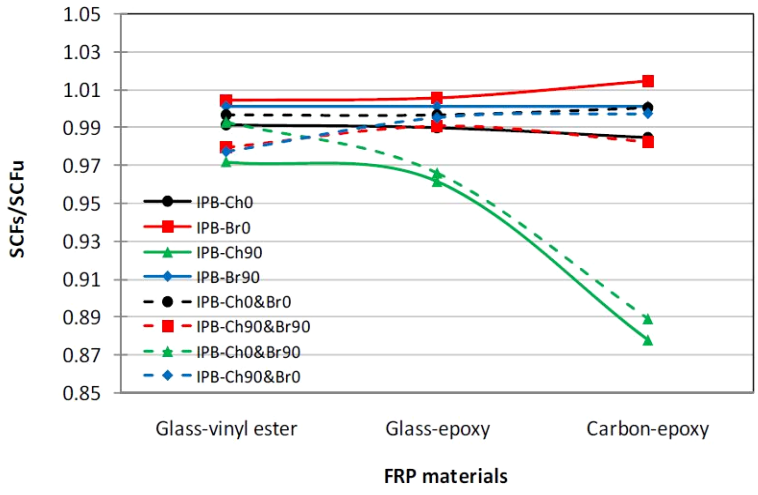

Figure 3: Ratio of SCF distribution in FRP strengthened tubular T-joint with different FRP materials to SCF distribution in un-strengthened joint under In-plane bending moment

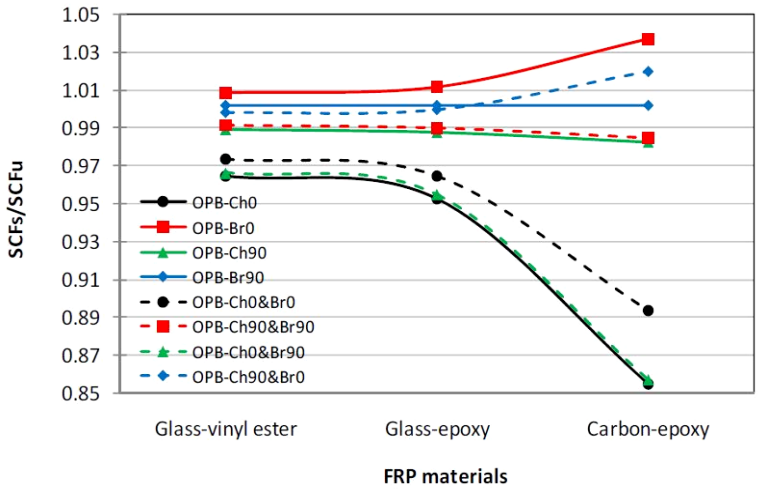

Figure 4: Ratio of SCF distribution in FRP strengthened tubular T-joint with different FRP materials to SCF distribution in un-strengthened joint under Out-of-plane bending moment

Having Figure 3 and Figure 4 along with the mechanical properties given in Table 1, one can find how the change in value of each mechanical property in two main extreme fiber orientations (0^o and 90^o) will affect the SCFs.

As depicted from Figure 3 and Figure 4, the effectiveness enhances by using stiffer composite material. Moreover, using carbon-epoxy material has higher effectiveness in comparison to the GFRP material on SCF reduction. Generally, it is revealed that among four different schemes of 0^o and 90^o fibers orientations for synthetic schemes (both chord and brace members are strengthened), when the chord member is strengthened with 0^o fibers in the FRP system and the brace member with 90^o (Ch0&Br90), the most reducing effect on SCF values is observed. As an example, using this scheme with Carbon-epoxy FRP material, SCFs are decreased by 11.2% under IPB loading and 14.6% under OPB loading.

Summary and Conclusions

In this research, SCF alteration at the Crown and Saddle positions of the Chord-Brace intersection area of the FRP strengthened T-joint under IPB and OPB moments was studied. Models were verified based on experimental data gathered from the JISSP project. The following conclusions were derived.

- Generally, more decrease in SCF values observed when stiffer FRP materials are used for strengthening.
- In case of IPB loading, the most decreasing effect on SCFs was observed when only the chord member is strengthened with 90^o orientation of fibers.
- In case of OPB loading, use of FRP wrapping with 0^o orientation of fibers only on the chord member has the most falling effect on SCFs. Brace strengthening has unfavorable results on SCFs in both IPB and OPB loading conditions, as when the fibers are in 0^o orientation, the worst effect was observed.
- Generally, results of SCFs for strengthening both chord and brace members stand between the results of individual chord or brace strengthening. As an interesting result, among the synthetic schemes (Strengthening both chord and brace members), when the chord and brace fibers are in 0^o and 90^o orientations respectively, the most effective result on downsizing the SCFs values was observed in both IPB and OPB loading conditions.
- Due to the better fatigue performance of CFRP materials in comparison to other composite materials such as GFRP, and based on the findings of this study, it is recommended to use CFRP composites as wrapping and strengthening material for fatigue life extension of tubular joints. Anyway, economical issues must be addressed.

Further numerical and experimental investigations would be necessary to achieve more understandings about SCF values in FRP strengthened joints.

References

[1] Jia, J., An efficient nonlinear dynamic approach for calculating wave induced fatigue damage of offshore structures and its industrial applications for lifetime extension, ‘‘Applied Ocean Research’’, Vol. 30, 189-198, 2008.

[2] API (American Petroleum Institute), Recommended practice for planning, designing and constructing fixed offshore platforms - working stress design, API RP 2A WSD, 22nd edition, 2014.

[3] Lesani, M., Bahaari, M.R., Shokrieh, M.M., Numerical investigation of FRP-strengthened tubular T-joints under axial compressive loads, ‘‘Composite Structures’’, Vol. 100, 71-78, 2013.

[4] Hollaway, L.C., Cadei, J., 2002, Progress in the technique of upgrading metallic structures with advanced polymer composites, ‘‘Progress in Structural Engineering and Materials’’, Vol. 4(2), 131-148.
[5] Zhao, X.L., Zhang, L., State of the art review on FRP strengthened steel structures, ‘‘Engineering Structures’’, Vol. 29(8), 1808-1823, 2007.
[6] Zhao, X.L., FRP strengthened metallic structures, ‘‘Thin Walled Structures’’, Special Issue, Vol. 47(10), 1019, 2009.
[7] Jiao, H., Zhao, X.L., CFRP strengthened butt-welded very high strength (VHS) circular steel tubes, ‘‘Thin-Walled Structures’’, Vol. 42(7), 963-978, 2004.
[8] Zhao, X.L., Fernando D., Al-Mahaidi R., CFRP strengthened RHS subjected to transverse end bearing force, ‘‘Engineering Structures’’, Vol. 28(11), 1555–1565, 2006.
[9] Lesani, M., Bahaari, M.R., Shokrieh, M.M., Experimental investigation of FRP-strengthened tubular T-joints under axial compressive loads, ‘‘Construction and Building Materials’’, Vol. 53, 243-252, 2014.
[10] Lesani, M., Bahaari, M.R., Shokrieh, M.M., FRP wrapping for the rehabilitation of Circular Hollow Section (CHS) tubular steel connections, ‘‘Thin-Walled Structures’’, Vol. 90, 216-234. 2015.
[11] Health and Safety Executive (UK), OTH 354: Stress concentration factors for simple tubular joints - assessment of existing and development of new parametric formulae, Prepared by Lloyd’s Register of Shipping, 1997.
[12] ABAQUS/CAE Standard user’s manual-Version 6.14-1, 2014.
[13] Ganesh, K., Naik, N.K., ‘‘Some strength studies on FRP laminates’’, Journal of Composite Structures, Vol. 24, pp. 51-58, 2005.
[14] AWS (American Welding Society), Structural welding code, AWS D 1.1:2010 (22nd Edition), Miami, FL (USA), American Welding Society, Inc, 2010.
[15] N’Diaye, A., Hariri, S., Pluvinage, G., Azari, Z., Stress concentration factor analysis for notched welded tubular T-joints, ‘‘International Journal of Fatigue’’, Vol. 29, 1554-1570, 2007.
[16] IIW-XV-E, International institute of welding sub-commission XV-E, recommended fatigue design procedure for welded hollow section joints, IIW Docs, XV-1035-99/XIII-1804-99, International Institute of Welding, France, 1999.

INTERNATIONAL JOURNAL OF
COASTAL & OFFSHORE ENGINEERING
IJCOE No. 1/Winter 2016 (7-13)

Dynamics modeling of the MoorMaster unit and investigate the interaction between the moored ship and the MoorMaster

Hassan Sayyaadi [1], Roya Rasa[2]

[1]*Professor, Center of Excellence in Hydrodynamics and Dynamics of Marine Vehicles/ Sharif University of Technology; Sayyaadi@sharif.edu*
[2]*M.Sc. Student, School of Mechanical Engineering/ Sharif University of Technology; rasa_roya@mech.sharif.edu*

ARTICLE INFO

Article History:
Received: 4 Oct. 2016
Accepted: 15 Mar. 2016

Keywords:
Mooring
MoorMaster units
Shore-based mooring
Vacuum based automated mooring technology
MoorMaster automated mooring

ABSTRACT

Developed mooring unit, the MoorMaster, which replaces conventional mooring lines is addressed here. The hydraulics of the system have a strong deducting effects on the motions of the moored ship. MoorMaster act in two different states. In first state; mechanism controls transfer mechanism to suitable position and joint with ship. Second state is passive mechanism state that lock in last position and the controller is passive so that springs and dampers appliance in mechanism carry passively apply forces from ship to mechanism. First; we defined state variables and According to the Lagrange equations, dynamics model of MoorMaster is extracted using Matlab Toolboxes and dynamics numerical simulations will be done. Then design a Controller to control the mechanism to stick to the vessel's body. Second state; investigate the interaction forces/moments in between the moored ship and the mechanism. have considered the simplest case, where the ship is located just under the MoorMaster force. Ship motion equations solved using Lagrange equations. And then design a controller that gives the ability to MoorMaster which exert forces and torques suitable in the freedom direction, per ship behavior. The results are given in a series of figures.

1. Introduction

Container ships should only make very small horizontal movements at the berth for efficient (off) loading of containers. This is especially a concern in ports directly facing the open ocean, where high swells at sea can cause harbor oscillations and low-frequency surge motions of the ship. On the other hand when a ship is moored at a quay wall or jetty, certain problems can occur:

- Mooring lines can break, which has resulted in (lethal) accidents in the past.
- Large motions of moored ships can result in inefficient handling of cargo by the cranes at the quay wall or jetty, especially in case of container handling.

The surge motion of a moored container ship is very critical. The surge amplitude should be smaller than 0.5 meter for efficient container handling (PIANC, 1995). Measurements at a container terminal port have shown that the surge motion of container ships was reduced from an amplitude of 1 meter to an amplitude in the order of 5 centimeters, while using MoorMaster™ units. MoorMaster units can offer a solution for both these problems. MoorMaster units consist of a vacuum pad which is attached to the ship hull. Hydraulic cylinders, connected to the vacuum pad, generate forces in the horizontal plane to control the horizontal motions of the moored ship. Four to twelve units are required to moor a ship depending on size of the ship, the cargo handling requirements and the local environmental conditions. Measurements have shown that ships moored with MoorMaster units move much less than ships moored with conventional mooring lines [1]. In 1999 Cavotec installed the first MoorMaster units at a ferry terminal in New Zeeland. Currently the units have been installed at about 10 locations in the world, mainly ferry terminals. The main advantage of MoorMaster units for a ferry terminal is quick mooring and instant release of the ship, without use of mooring lines [1].

Apart from a quick fastening of the vessel using vacuum pads, the hydraulics of the system showed to have a strong reducing effect on the motions of the moored ship. Therewith, MoorMaster™ units include a method to reduce (large) vessel motions and reduce operational downtime, which makes them suitable for mooring large container ships. MoorMaster units

control horizontal motions of moored ship better than conventional mooring lines, because:

- MoorMaster units are stiff and generate efficient forces in magnitude and direction to control ship motions. Forces generated by mooring lines only respond to (relatively large) displacements of the moored ship.
- The MoorMaster force is being generated for 100% in the horizontal plane. Only a percentage of the force generated by a mooring line (40%-80%, depending on the angle of the mooring line) acts in the horizontal plane. The feasibility of MoorMaster units mainly depends on environmental conditions and operational requirements in a port and is eventually an economic consideration.

Possible economic advantages of MoorMaster units compared to conventional mooring lines are:

- Increasing efficiency of cargo handling and extending the operational period of cargo handling, because of higher reduction of ship motions.

MoorMaster units can allow higher waves in the harbor basin, while still keeping the ship motions within the motion criteria for efficient cargo handling. This can result in considerable savings on breakwaters.

Possible disadvantages of using MoorMaster units, compared to using conventional mooring lines are:

- Higher capital costs (of the units only, not considering possible cost savings of more efficient operations and reduced length of breakwaters).
- High maintenance level, especially in a saline environment of a sea port.
- Higher power consumption.

In here studied on the operation mechanism of MoorMaster units. With attend to a MoorMaster unit can say that mechanism action in two states, here in two step explained the operation mechanism of MoorMaster units. In first step dynamics model of MoorMaster is extracted. And in second step Obtain applied forces and moments on one MoorMaster from ship.

Modeling the operating mechanism is an important tool for port engineers to make a port design, which provides acceptable conditions to handle the cargo efficiently.

Step1: explain the operation mechanism of MoorMaster and dynamics simulation

Dynamics modeling of the mechanism it was shown in fig1 is addressed here. Defined state variables and According to the Lagrange equations, dynamics model of MoorMaster is extracted using Matlab Toolboxes and dynamics numerical simulations will be done. Then design a Controller to control the mechanism to stick to the vessel's body.

Extracted dynamics modeling of this mechanism is shown in fig2. Its characteristic is represent in table1.

Table1- Extracted dynamics modeling characteristic

m_1	100kg	l_6	0.3m
m_2	100kg	l_7	0.2m
m_3	40kg	a	0.3m
l_0	1.5m	b	0.1m
l_1	1.5m	c	0.3m
l_2	1.3m	k	500N/m
l_3	0.4m	I	$m_1 {l_2}^2/_2$
l_4	0.35m	x-final	1m
l_5	0.7m	θ_1-final	$\pi/_2$ rad

Figure1 -Moormaster unit, a commercial type [1]

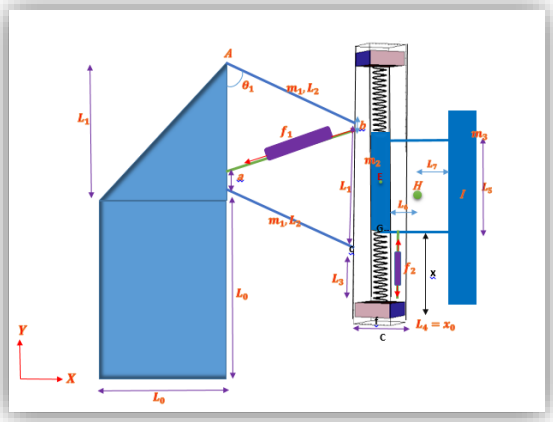

Figure2- Extracted dynamics modeling of MoorMaster

Angular motion θ_1 and vertical displacement x are to be considered as state variables for actuating the MoorMaster mechanism and the other depicted parameters are constant values in the mechanism. These two input variables are actuated via two hydraulic jacks which can exert jack forces (f_1 andf_2). f_1 Is the actuating force to derive $\theta_1$and f_2 is similarly for x.

According to the fig2 kinetic energy of the system and potential energy of the system are:

$$T = \frac{1}{2}m_1 {V_{CG_1}}^2 + \frac{1}{2}m_1 {V_D}^2 + \frac{1}{2}\, I\, \dot{\theta}_1 + \frac{1}{2}\, I\, {\dot{\theta}_1}^2 + \frac{1}{2}m_2 {V_E}^2 + \frac{1}{2}m_3 {V_H}^2 \quad (1)$$

$$V = m_1 g V_{CG_1}(2) + m_1 g V_D(2) + m_1 g V_E(2) + m_1 g V_H(2) + \frac{1}{2}\, Kx^2 + \frac{1}{2}\, Kx^2 \quad (2)$$

Now dynamics analysis the mechanism by using matrix Lagrange equations [2].

$$\frac{d}{dt}\left(\frac{\partial L}{\partial\{\dot{q}_i\}}\right) - \frac{\partial L}{\delta\{q_i\}} = \{Q_i\} \quad (3)$$

q is Generalized coordinates and L is the Lagrangian and Q is matrix of forces and torques.

According to the Lagrange equations, dynamics model of MoorMaster is extracted using Toolboxes Matlab2013 software. Dynamics numerical simulations to verify equations. Fig3 is shown dynamics energy at time after numerical simulations (while the mechanism not stick to the vessel's body and no force and moment apply to the MoorMaster).
According to fig3 E is in acceptable range, therefore Extracted dynamics is suitable. Because the total energy remained conservative.

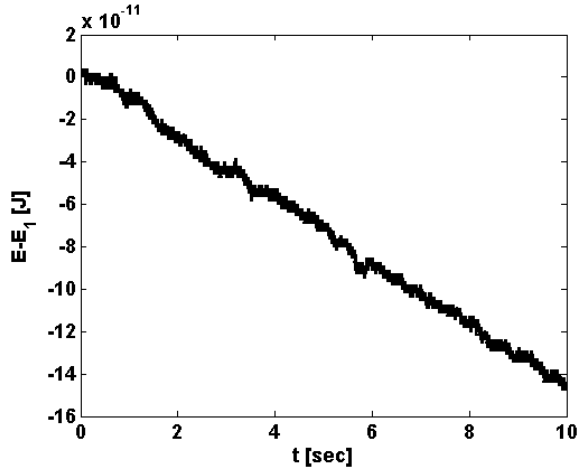

Figure3 - dynamics energy at time

Now it is needed to control the mechanism of MoorMaster to stick to the vessel's body. This is a nonlinear dynamic system with two control input u_1 and $u_2$in each of the above mentioned jacks which were shown with f_1 andf_2. The adopted method for dynamic control is based on 'input-output Linearization' [3].
Applied control law is:

$$\ddot{q} = u = \ddot{q}_d - 2\lambda\dot{\tilde{q}} - \lambda^2\tilde{q} \quad (4)$$
$$that\ \ \tilde{q} = q - q_d\ , \dot{q} = \dot{q} - \dot{q_d}$$

In this system we have:

$$[M_L]\{\ddot{q}\} + \{B_L\} = \{Q\} \implies \{Q\} = [C]\{u\} \quad (5)$$

$$\{Q\} - \{B_L\} = [M_L](\{V\}) \implies \{Q\} = \{B_L\} + [M_L](\{V\}) \implies \{V\} = \{\ddot{q}\} \quad (6)$$

With apply I/O law:

$$\{V\} = \{\ddot{q}_d\} - 2\begin{Bmatrix} \lambda_1\dot{\tilde{q}}_1 \\ . \\ : \\ \lambda_m\dot{\tilde{q}}_m \end{Bmatrix} - \begin{Bmatrix} {\lambda_1}^2\tilde{q}_1 \\ . \\ : \\ {\lambda_m}^2\tilde{q}_m \end{Bmatrix}$$

$$\Longrightarrow \begin{cases} \ddot{\tilde{q}}_1 + 2\lambda_1\dot{\tilde{q}}_1 + {\lambda_1}^2\tilde{q}_1 = 0 \\ \vdots \\ . \\ \ddot{\tilde{q}_m} + 2\lambda_m\dot{\tilde{q}}_m + {\lambda_m}^2\tilde{q}_m = 0 \end{cases} \quad (7)$$

From (5) and (7);

$$\{u\} = [C]^{-1}\{Q\} = [C]^{-1}\big(\{B_L\} + [M_L](\{V\})\big) \quad (8)$$

By substituting numerical values of system parameters according to Table1, and initial condition $x = 1.5 - 0.1$ (m), and $\theta_1 = {}^{\pi}/_{3}$ (rad), the controller outputs and Tracking error of staste variables will be derived. That are shown in fig4 and fig5.

Results and discussions

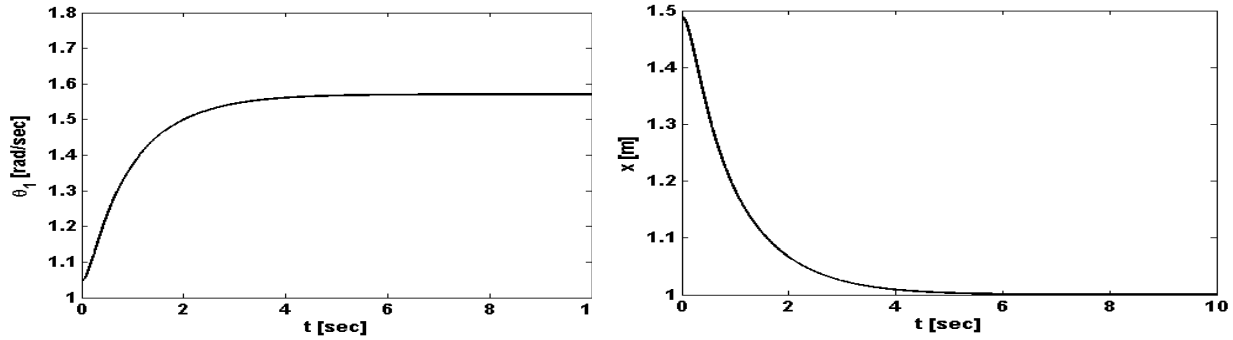

Figure 4 - staste variables

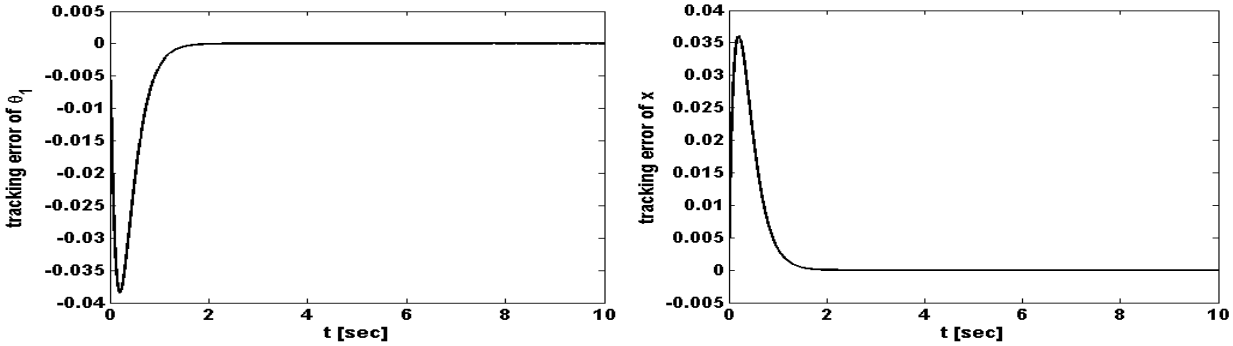

Figure 5 - Tracking error of staste variables

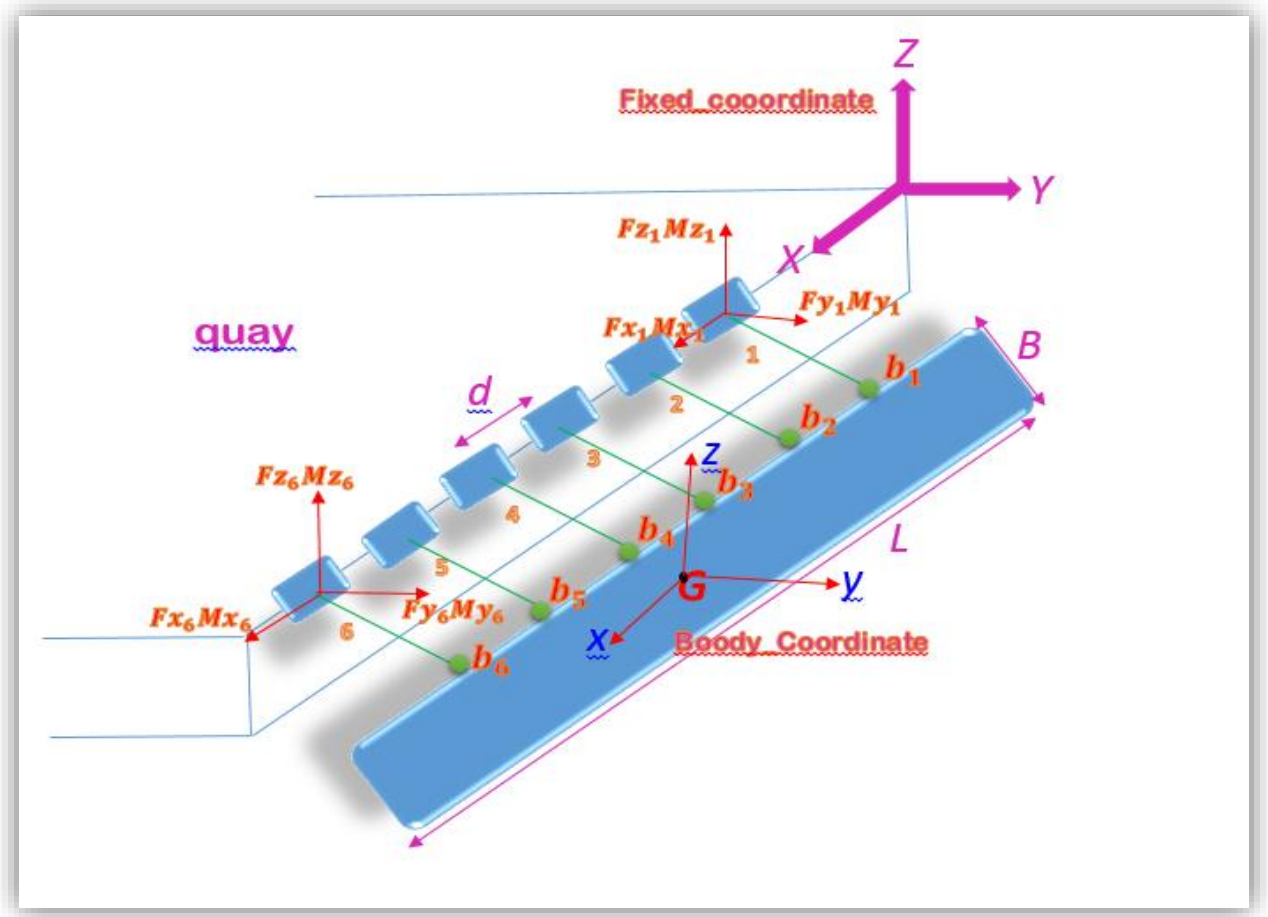

Figure 6 - A schematic of the moored ship connected to 6 MoorMaster units

Table2- Ship characteristics under review

(length) L	100m	g	9.81
B)width(	30	I_{XX}	225000
d)MoorMasters longitudinal distance from each other(	14	I_{YY}	22500000
a)Vertical distance of the center of mass to the connection point MoorMasters(	5	I_{ZZ}	22500
H)Height(	20	Δ	1096087.3

According to fig4 and fig5 numerical simulations results show that control law used up was acceptable, because in less than one second achieve to perfect tracking error. And system state variables smoothly achieved to the final value.

Step2: explain the investigate the interaction between the moored ship and the MoorMaster

It is needed to investigate the interaction forces/moments in between the moored ship and the mechanism. First, we have considered the simplest case, where the ship is isolated and located just under the MoorMaster force. Ship motion equations solved using Lagrange equations. And then design a controller that gives the ability to MoorMaster which exert forces and torques suitable in the freedom direction of the floating to ship, per ship behavior. 6 arbitrarily MoorMaster units for typical ship is intended for modeling. As can be seen in the below figure (fig6). In fig6 is shown a schematic of the moored ship connected to 6 MoorMaster units. That Ship characteristics under review is represent in table2.

To describe the locations of system components is need to introduce two coordinate systems, which is a fixed coordinate system, on the edge of the quay is considered (X,Y,Z) and the other is Moving coordinate systems (body coordinate) that is located in the center of gravity of ships(x, y, z). With follow of rotatory Euler angles pattern, coordinate system (x, y, z) can be level to coordinate system (X, Y, Z). rotatory pattern, respectively consist of; the first rotation (precession) The amount of angle ψ around axis z , the second rotation (Nutation) The amount of angle θ around axis new y, The third rotation (Spin) The amount of angle ϕ around axis new z. Which combines three rotation pattern, gives converting coordinates system (x, y, z) to (X, Y, Z) [2].

For this ship with 6 degree of freedom, 6 generalized coordinates have to be defined, according to Euler angles [2] and definition coordinate systems. That respectively consist of;

$$q_1 = X, q_2 = Y, q_3 = Z, q_4 = \psi, q_5 = \theta, q_6 = \phi \qquad (9)$$

To solve equations need to use the Lagrange equations in the matrix form (equation 3).

Due to the symmetry plane of the draft on ships and to simplify problems, consider inertia matrix (I) polarity. now can kinetic and potential energy values calculated as a function of generalized coordinates;

$$\begin{aligned} T = \frac{1}{2}M\left(\dot{q_1}^2 + \dot{q_2}^2 + \dot{q_3}^2\right) &+ \frac{1}{2}I_{xx}\left(\dot{q_4}^2(\sin q_5)^2(\cos q_6)^2 + \dot{q_5}^2(\sin q_6)^2\right) \\ &+ \frac{1}{2}I_{yy}\left(\dot{q_4}^2(\sin q_5)^2(\sin q_6)^2 + \dot{q_5}^2(\cos q_6)^2\right) \\ &+ \frac{1}{2}I_{zz}\left(\dot{q_4}^2(\cos q_5)^2 + \dot{q_6}^2\right) \qquad (10) \end{aligned}$$

$$V = -Mgq_3 \qquad (11)$$

That Lagrangian equation form used for this system are as follows:

$$(M\_L)\ddot{q} + (B\_L) = Q = C * F \qquad (12)$$

That M_L , B_L are Lagrangian matrix. Q is matrix of forces and torques are applied to MoorMasters and as unknowns, C is constant coefficient, F is applied forces and moments on the MoorMaster matrix. F can be expressed as follows:

$$F = \left[F_{x_1}, F_{y_1}, F_{z_1}, F_{x_2}, F_{y_2}, F_{z_2}, F_{x_3}, F_{y_3}, F_{z_3}, F_{x_4}, F_{y_4}, F_{z_4}, F_{x_5}, F_{y_5}, F_{z_5}, F_{x_6}, F_{y_6}, F_{z_6}, M_{x_1}, M_{y_1}, M_{z_1}, M_{x_2}, M_{y_2}, M_{z_2}, M_{x_3}, M_{y_3}, M_{z_3}, M_{x_4}, M_{y_4}, M_{z_4}, M_{x_5}, M_{y_5}, M_{z_5}, M_{x_6}, M_{y_6}, M_{z_6}\right]^T \qquad (13)$$

Due to the dynamic floating and connection MoorMaster to the ship, from any MoorMaster three forces and three moments is applied, in three direction of coordinate system attached to the center of mass (fig6).

$$\begin{cases} F_{y_i} \approx \text{Sawy motion} \\ F_{z_i} \approx \text{heave motion} \\ F_{x_i} \approx \text{Surge motion} \end{cases}, \begin{cases} M_{y_i} \approx \text{Pitch motion} \\ M_{z_i} \approx \text{Yaw motion} \\ M_{x_i} \approx \text{Roll motion} \end{cases}$$

All components must be transmitted to the coordinate system fixed with using transmission matrix [2].

To understand that how much forces and torque should be carried MoorMasters for each movement of the ship. To this purpose should be using a proportional control law to this system, Here has been

used the linearization control law in put _ Out put based on the tracking error [3].
In this system we have:

$$(M\_L)\ddot{q} + (B\_L) = C * F \implies (M_L)\ddot{q} = (B_L) + C * F = Mv \quad (14)$$

Applied control law is:

$$\ddot{q} = v = \ddot{q}_d - P\dot{\tilde{q}} - Q\tilde{q} \quad (15)$$

To predict the forces and torques acting on the MoorMaster units, applied to the system any desired movement of the ship as $q_d = q\ desired$ then Obtains Proportional forces and torques based on. Here for the first step a linear frequency has been considered as follows.

$$q_{1_d} = 0.1 \sin t \quad (16)$$

To simplify the problem, the frequency moving ship in other directions is zero, [except the coordinates q_5 that due $\cos(q_5)$ in the denominator of one the term of the equation of motion appeared; should not to be 0 and π, which arbitrary $dq_5 = \frac{\pi}{3}$ is considered]. Initial condition of the system, also expressed based on the q_d .

Results and discussions

Calculate equations using numerical solution, for numerical solution can use matlab2013 numerical solvers, as "Ode45". Equation is solved for a ship with the specifications Table2, and the results of simulations and tracking error diagrams of state variables have been extracted in fig7.

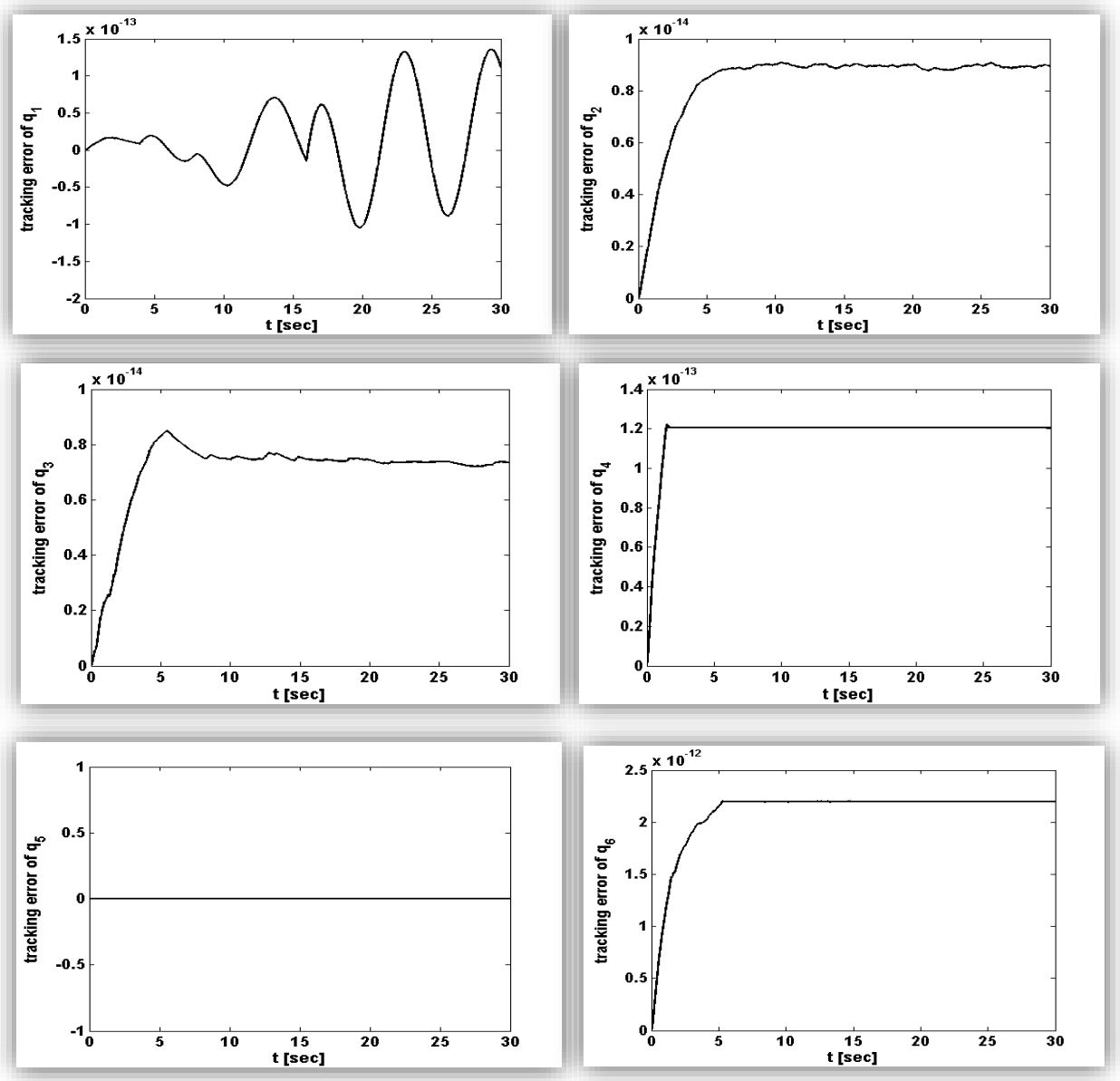

Figure 7 - tracking error diagrams of state variables

Graphs in fig7 Show that in the second state also in less than a second perfect tracking is smoothly achieved. It means that the Extracted forces and torques are applied forces and torques to MoorMasters.

Based on simulation results, we see that the proposed control scheme shows Perfect tracking behavior. And the error is in the proper range, so can say that if the ship do a longitudinal frequency as $0.1 \sin t$, for example first MoorMaster unit must bear the below forces and torques. (fig8)

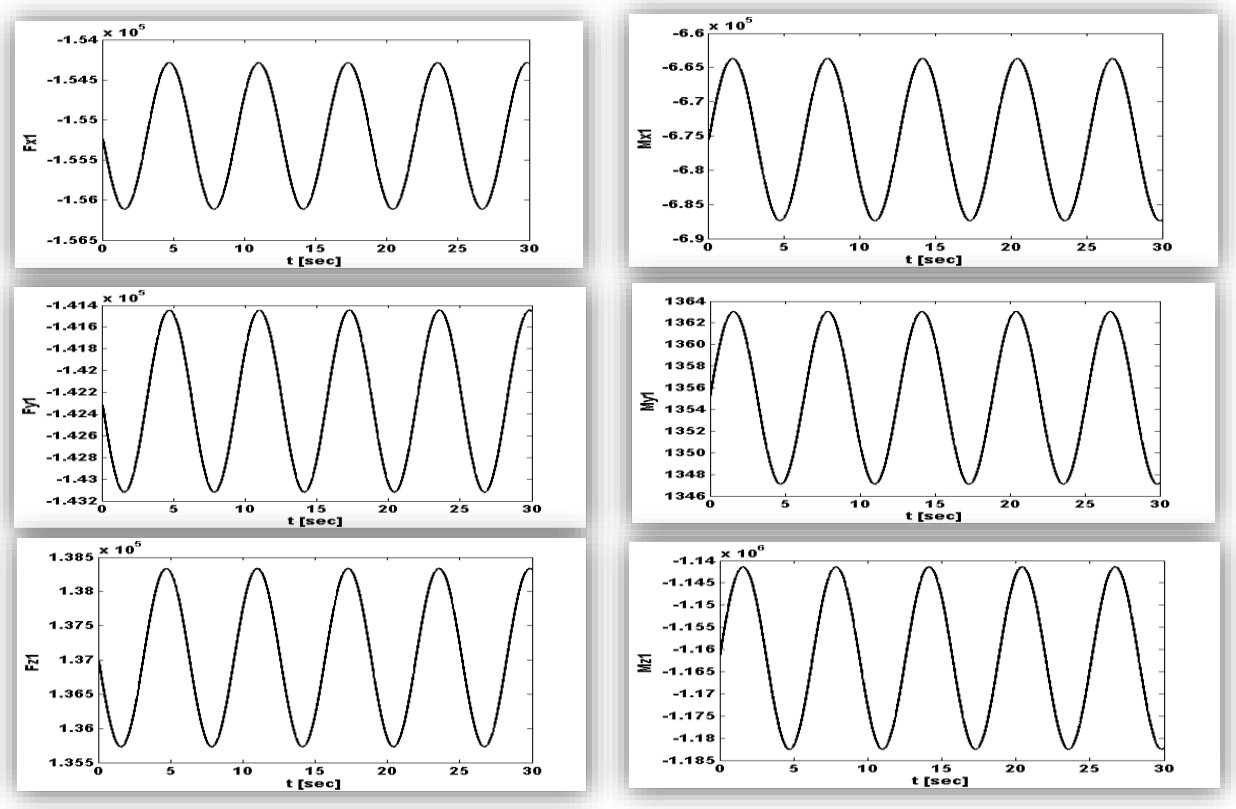

1Figure8- first MoorMaster unit forces and torques

Conclusions

In this paper Considered two state for MoorMaster operation. In first state; mechanism controls transfer mechanism to suitable position and joint with ship, results shown in less than a second perfect tracking is smoothly achieved, It is a well extraction system dynamics. Second state is passive mechanism state that lock in last position and the controller is passive so that springs and dampers appliance in mechanism carry passively apply forces from ship to mechanism. In fact, Obtain applied forces and moments is the aim of the second state. Which enables the design engineers performing better design with the correct prediction of the MoorMaster behavior for the different of ships when loading and unloading at the quay.

One can also consider the different frequency motion of ship as desired trajectory, then extract the forces and torques.

References

[1] de Bont1, W. van der Molen2, J. van der Lem3, H. Ligteringen4, D. Mühlestein5 and M. Howie., 2010. "Calculations of the motions of a ship moored with moormaster™ units". Port Infrastructure Seminar.

[2] Jerry H. Ginsberg., 1999. Advanced Engineering Dynamics. Cambridge University Press, page 266-271.

[3] W Lohmiller, JJE Slotine, 1998. On contraction analysis for non-linear systems. Automatic, Elsevier.

[4] Mark W. Spong, Seth Hutchinson, and M. Vidyasagar, (2006), Robot Modeling and Control, John wiley and sons, page 140-141.

[5] https://www.scribd.com/doc/285169068/MoorMaster-Reference-List-Lres-May-2011

INTERNATIONAL JOURNAL OF
COASTAL & OFFSHORE ENGINEERING .IJCOE No. 1/Winter 2016 (15-23)

Engineering Critical Assessment of Offshore Pipelines under Operational Loading Phase According to BS 7910 Guideline

Seyed Mohammad Hossein Sharifi[1], Mehran Kaveh[2], Hamed Saeidi Googarchin[3]

[1]Assisstant Professor, Faculty of Marine Science, Petroleum University of Technology, Abadan, Iran; Sharifi@put.ac.ir
[2]M.Sc Student, Faculty of Marine Science, Petroleum University of Technology, Abadan, Iran; MKaveh@put.ac.ir
[3] Assistant Professor, School of Automotive Engineering, Iran University of Science and Technology, Tehran, Iran; HSaeidi@iust.ac.ir

ARTICLE INFO

Article History:
Received: 15 Nov. 2016
Accepted: 15 Mar. 2016

Keywords:
Engineering critical assessment (ECA)
offshore pipeline
surface cracks
girth weld misalignment, BS 7910

ABSTRACT

Offshore pipelines are an efficient long-distance transportation method for oil and gas. These are usually constructed by the use of girth welds, while welds may naturally contain flaws. Hence, it is essential to inspect the fracture response of girth welds in order to check the structural integrity of the pipeline. One of the guidelines that is using wide spread for investigating the fracture response of steel structures is BS 7910 which is based on Engineering Critical Assessment (ECA) method. In this paper Engineering Critical Assessment (ECA) of offshore pipeline girth welds is done according to BS 7910 through Crackwise software and the influence of several parameters on ECA is presented. It is concluded that Influence of misalignment on axial internal surface flaws is more significant than on axial external flaws. Furthermore it is observed that internal surface flaws have always larger values for tolerable defect heights than external surface cracks. In addition, circumferential surface flaws have evermore larger amount of acceptance level in defect heights than axial flaws.

1. Introduction

In order to transport oil and gas e.g. from the platforms to land-based terminals, offshore pipelines are utilized which are usually composed of a number of short pipes joined by welding. The girth welds may contain weld imperfections of certain size (height and length) at specific location along the longitudinal direction of the weld. [1]. Therefore, it is important to find a suitable fracture assessment procedure for welded pipeline and know how these eventual cracks develop in order to assess the structural integrity of the pipelines [2]. For this means, two methods were introduced which are quality control and Fitness-For-Purpose (FFP) approaches. Quality control approach usually gives both arbitrary and conservative levels for acceptance; however FFP procedure make the acceptance levels very less conservative by providing the conditions to cause failures in structures are not reached[3]. Engineering Critical Assessment (ECA) is a FFP procedure which is based on fracture mechanics principles. It was introduced by Kumar et al [4] in 1981. They proposed an analytical methodology for computing crack driving force based on J-Integral which was published by Electric Power Research Institute (EPRI). The EPRI equations for fully plastic condition suppose a simple power law for the material's plastic stress-strain curve. Anisworth modified the EPRI relationships in order to make it more representative of the flow behavior of real materials. He defined reference stress approach and substituted it to the plastic component of EPRI procedure to characterize the possibility of plastic collapse alongside fracture failure [5]. With additional simplifications and modifications to the reference stress approach, BS7910:2005[6] express it in terms of a Failure Assessment Diagram (FAD). At the moment, this regulation is widely used in order to determine defect acceptance criterion in steel structures.

First attempts on ECA analysis in accordance with BS 7910 code have been made by Darcis et al [7]. They studied fracture assessment process in fillet-welded joints where cracks emanate from the weld toe. Pysarsky and his colleagues [8] investigated ECA analysis of high strength steel pipeline girth welds which are subjected to plastic axial loading. Several studies have been performed in order to compare different methods of ECA analysis. Permana [9]

performed a case study on ECA analysis of a pipeline girth weld during reeling installation and compare BS 7910 code with direct finite element. Although BS 7910 tends to be conservative for long crack lengths compared to finite element analysis, it shows less conservative critical crack sizes in the region of short cracks. Smith and Pisarski [10] compare API 1104-Appendix A and BS 7910 FAD procedure with and without residual stress. Larger flaws are allowed by the BS 7910 procedure compared with API 1104 procedure, irrespective of whether the safety factor on flaw length is included or not in the API 1104 assessment. Also, Larrosa and Anisworth [11] showed the differences in ECA results which are assessed by the API 579, the UK nuclear industry standard for fracture assessment (R6), and BS 7910 procedures. They revealed that BS 7910 has larger plastic collapse limitation compare to the other codes.

However, few literatures contribute to investigate the effect of various parameters on ECA of offshore pipelines in accordance with BS 7910. Holtman [12] focused on examining the fracture behavior of offshore pipeline steel in sour environment (containing water and hydrogen sulphide). Wei and Handley [13] presented the effects of bi-axial stressing (internal pressure plus external axial loading) on ECA analysis of plate and cylinder containing surface cracks. Recently, Bonara et al [14] investigated the ECA procedure to assess CRA welds for clad and lined pipe material in bi-metallic girth weld joints. As an extension, this study is aimed to investigate the influence of axial misalignment in girth welds and ductile tearing on engineering critical assessment of girth welded offshore pipelines under operational loading phase based on BS 7910 guideline for various flaw geometries.

In this paper, influence of various parameters on engineering critical assessment of offshore pipelines is performed. Accordingly, a brief overview of BS7910 and theoretical background of engineering critical assessment method is provided; afterward, geometrical configurations, mechanical properties of pipeline materials, and loading scenarios are described in details. Influence of axial misalignment in girth welds and ductile tearing on ECA analysis of offshore pipeline in various flawed geometries is presented based on BS 7910 code. Finally, summary of results and conclusions are given in the last section.

1. BS 7910

Because workmanship standards settle totally specific rules for allowable lengths of slag inclusion and density of porosity, a large amount of repair work is carried out for innocuous planar flaws such as cracks based on these codes. It has been estimated that such unnecessary repairs may add as much as 10% to construction costs [15]. In this order, British Standards Institution set up a logical acceptance standard which was both safer and more economical than the traditional workmanship acceptance standards.

In BS 7910: 2013[3], there are three levels, available for a fracture assessment. The Level 1 which is called simplified assessment procedure is based on a conservative Failure Assessment Diagram (FAD) applicable when the data on the materials properties is limited. The Level 1 FAD has Kr, Sr co-ordinates, where Kr is the ratio of applied crack driving force to fracture toughness and Sr the ratio of applied stress to flow strength where the flow strength is mean of yield and tensile strength hence including some plasticity. For the cases where single-value measurements of fracture toughness are available level 2 which is named normal assessment method is used. Further there are two assessment strategies: Level 2A and Level 2B. When material specific full stress–strain information is available, Level 2B is utilized based on reference stress solution. Level 3 is similar as level 2 with the exception that is appropriate for ductile materials showing tearing mode of failure with Level 3A and 3B dependent on the type of stress-strain data available. A typical figure of level 2 FAD is shown in figure 1.

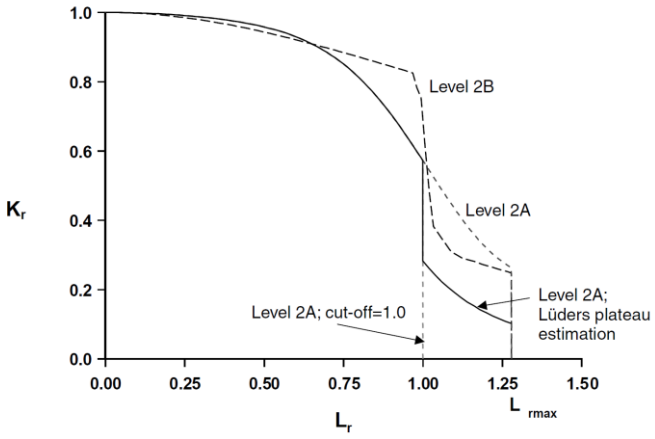

Figure 1- BS 7910 level 2 failure assessment diagram [3]

According to BS7910 level 2B, a flaw can be accepted when the following equation is satisfied:

$$K_r \le \left(\frac{E \times \varepsilon_{ref}}{YS \times L_r} + \frac{{L_r}^3 \times YS}{2 \times E \times \varepsilon_{ref}} \right)^{-1/2} \qquad (1)$$

In the above equations, $K_r = K_I / K_{mat}$ is fracture ratio, σ_{ref} is reference stress, ε_{ref} is the true strain obtained from the uni-axial tensile stress-strain curve at reference stress, $L_r = \sigma_{ref} / YS$ is load ratio and $L_{r(max)} = UTS + YS / 2YS$ is cut-off value, E is the Young's modulus. The first term in equation 1 considers both the limiting elastic and fully plastic behaviors. The second term determines the response

in between these two limits where the general behavior is elastic but fracture parameter exceeds its elastic value, and a minor plasticity correction is supply by this term.

2. Methodology

In order to perform engineering critical assessment of offshore pipeline in accordance with BS 7910 guideline, Crackwise software [16] is utilized. Crackwise is a software which is used to compute multiple parametric equations, propagating flaws in ductile tearing, calculation of limiting conditions (for example, the maximum tolerable flaw size in a structure under given conditions), reporting, editing and archiving such complex calculations. Input values of this software for current study are as fallows.

2.1. Geometrical Configuration

The outer radius of pipeline is 203.2 mm, and the average wall thickness is 20.4 mm. The length of the pipe is considered three times as long as the outer diameter**.** Two types of cracks are proposed which are including external surface and internal surface flaws. These defects are located in axial and circumferential direction along the pipeline length and girth weld, respectively. Figure 2 shows the pipeline cross section alongside with various crack types used in this paper. "r_O" represent outer radius of the pipeline, "B" shows average wall thickness, the crack height is symbolized as "a", and "2c" representing the crack length and "p" showing crack ligament height in embedded flaws.

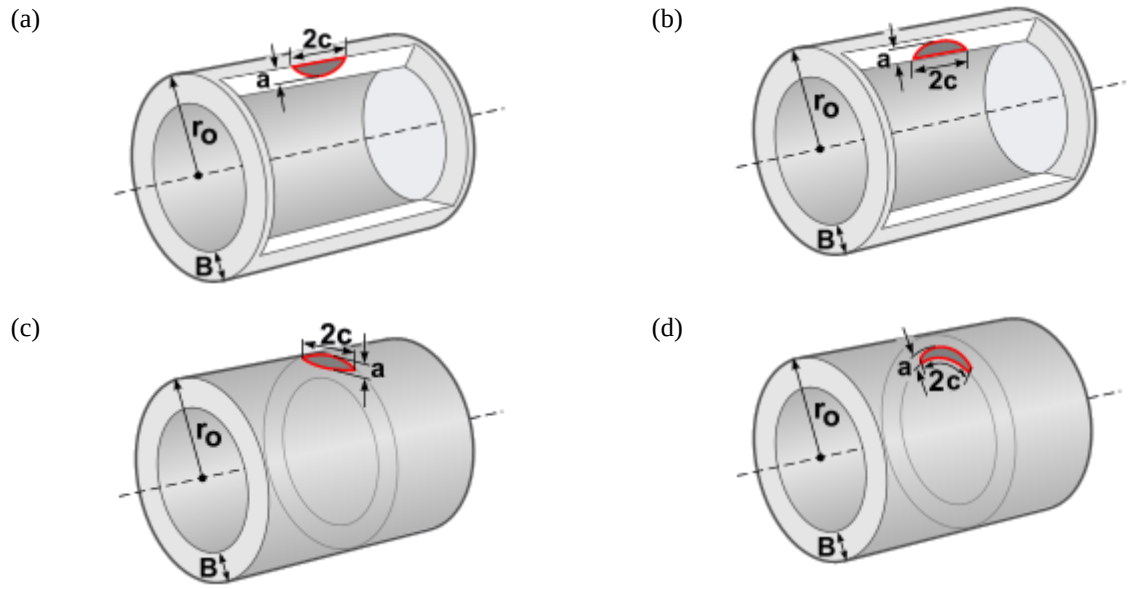

Figure 2- Crack geometries used in current study: (a) axial external surface, (b) axial internal surface, (c) circumferential external surface, (d) Circumferential internal surface flaws [16]

2.2. Material Properties

Two stress-strain curve equations which are widely used for modeling engineering materials are Ramberg-Osgood equation and the CSA Z662 [17] equation. CSA Z662 in contrast to Ramberg-Osgood equation provides the relationship between the stress and strain as mentioned in equation 2:

$$\varepsilon = \frac{\sigma}{E} + (0.005 - \frac{YS}{E})(\frac{\sigma}{YS})^n \qquad (2)$$

where E is young modules, YS is the yield stress at 0.5% strain and n is the strain hardening exponent of the CSA equation. Equation 3 determines a unique n for any given set of yield stress (YS), Ultimate Tensile Strength (UTS), and uniform Elongation (uEL). Hence, a full stress-strain curve can be determined uniquely by the CSA equation for the input YS, UTS, and uEL. Based on the aforementioned observations, in this paper the CSA Z662 equation is selected to produce the full stress-strain curves (option 2 in Crackwise FAD failure locus) in all models. Table 1 shows the input information for generating stress-strain curve which is mentioned in reference [18].

$$n = \ln(\frac{uEL - UTS/YS}{0.005 - YS/E}) \Big/ \ln(\frac{UTS}{YS}) \qquad (3)$$

Table 1-Mechanical properties used in pipeline [18]

Pipe	YS (MPa)	UTS (MPa)	E (GPa)	uEL (mm/mm)	n	Poisson's ratio
API-5L-X65	545	592	207	0.0816	39.25	0.3

2.3. Toughness

Fracture toughness is described by single-value measurements (K_I, J-Integral, CTOD) on level 2 assessment and expressed in terms of an resistance curve (J-Δa or CTOD-Δa) on level 3 assessment method. Hence, in this paper for level 2 assessment K_I is equal to 338 MPa.$\sqrt{m}$ [18]. Based on DNV-RP-108 [19], the resistance curves shall be established as a lower bound curve for the experimental results. Often a curve of the form $J=x^* \Delta a^m$ fits the data well. X=713.43 and m= 0.5 is considered here as in reference [18].

2.4. Loading Scenarios

A pipeline is laid on the seabed will be inclined to expand longitudinally because of temperature and pressure differential along the pipeline path. If the expansion is constrained by the frictional resistance force between pipeline and soil, then an axial compressive load which is called effective axial force will be exerted on the pipeline (High Pressure/ High Temperature condition) [20]. The effective axial force increases from pipeline end until it reaches its maximum at the point of full axial constraint. The effective axial force in fully constrained condition during operation can be calculated as a result of end-cap effect, Poisson's effect, thermal and residual lay tension [21]. For design purposes, according to Subsea7 documentations [22] the residual lay tension may be assumed to be negligible. Therefore, full constrained effective axial force is given as in equation 4:

$$N_{eff}(x) = H - \left(N_{end-cap(x)} + N_{poisson} + N_{thermal}\right) \qquad (4)$$

Where H is residual lay tension, $N_{end-cap(x)} = \Delta P.A_i$ is end-cap effect, $N_{poisson(x)} = -\nu \frac{\Delta P.D_i.A_s}{2t}$ is Poisson's effect, and $N_{thermal(x)} = -E.A_s.\alpha.\Delta T$ is thermal effect.

Largest effective axial force at anchor point is occurred when the fully constrained effective driving force equals the soil frictional force. Friction force induced by pipeline-soil interaction is as in equation 5.

$$S_{f,max} = \mu_{max,axial} \times W_{submerged} \times \frac{L}{2} \qquad (5)$$

In the above equation, $\mu_{max,axial}$ is maximum axial frictional factor, L is pipeline length, $W_{submerged}$ is the submerged weight which is calculated with respect to the pipeline data's. In this paper, $\mu_{max,axial}$=0.45, $W_{submerged}$=3.345 KN/m, and L=10 km are assumed according to reference [22]. Effective axial force along the pipeline and anchor point is shown in figure 3.

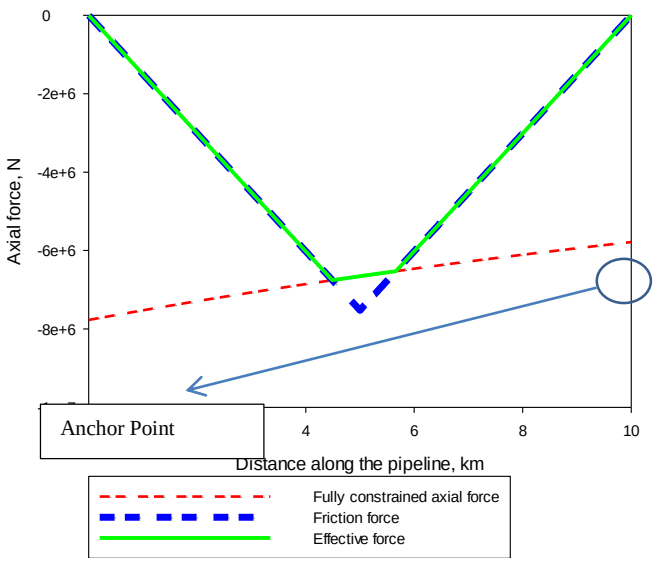

Figure 3- Effective axial force along the pipeline length

According to BS 7910, the stresses that will be considered in the analysis are primary and secondary stresses. The primary stress is stresses that could contribute to plastic collapse. They include all stresses appearing from internal pressure and external loads. Thermal and residual stresses are usually classified as secondary stresses. A significant characteristic of secondary stresses is that they do not, cause to plastic collapse. However, both primary and secondary stresses can contribute to failure by fracture. The stresses are separated into membrane and bending primary and secondary components. In this study, primary membrane stress due to High Pressure/ High Temperature condition is assumed as 288 MPa which is the largest stress occurred at anchor point along the pipeline length. Primary bending stress component that is induced by misalignment in the pipeline is calculated using Stress Concentration Factor (SCF) in association with Neuber's rule [23]. 3 different bending stresses are considered in order to investigate the influence of misalignment on fracture response of offshore pipeline. The base case is performed without misalignment. Afterward, it was compared with alternative eccentricities of 1 mm and 2 mm. Since offshore pipes had appropriate dimensional tolerances, 1 mm misalignment might be more realistic in many cases. However, 2mm misalignment is supposed to have maximum value along the girth weld direction [24]. According to annex Q of BS7910 with considering non-uniform residual stress distribution, secondary membrane and bending stress will be equal to 591.79 and 78.67 MPa.

2.5. Crackwise Modeling

The flowchart which is shown in figure 4 describes the crackwise analysis sequence. For ECA analysis in

level 2B and 3B, full stress-strain data for the material are needed. Yield and tensile strength, and modulus of elasticity should be determined along with adequate co-ordinate stress/strain points to define the curve. The cut-off limit is to prevent localized plastic collapse and it is set at the point at which $L_r = L_{r,max}$ where [3]:

$$L_{r,max} = \frac{YS + UTS}{2 \times YS} \quad (6)$$

The load ratio L_r is calculated from the following equation [3]:

$$L_r = \frac{\sigma_{ref}}{YS} \quad (7)$$

Where, σ_{ref} is obtained from an appropriate reference stress solution as outlined in BS 7910. Fracture ratio is calculated from the following equation [3]:

$$K_r = \frac{K_I}{K_{mat}} + \rho \quad (8)$$

Where ρ is plasticity correction factor and is necessary to allow for interaction of the primary and secondary stress contributions, and the applied stress intensity factor, K_I, has the following general form [3]:

$$K_I = (Y\sigma)\sqrt{(\pi a)} \quad (9)$$

$$(Y\sigma) = (Y\sigma)_P + (Y\sigma)_Q \quad (10)$$

Where $(Y\sigma)_P$ and $(Y\sigma)_Q$ represent contributions from primary and secondary stresses, respectively.

$$(Y\sigma)_P = Mf_w(k_{tm}M_mP_m + k_{tb}M_b(P_b + (k_m - 1)P_m \quad (11)$$

$$(Y\sigma)_Q = M_mQ_m + M_bQ_b \quad (12)$$

Where,
F_W = Finite width correction factor,
$K_{tm/tb}$ = Membrane/bending stress SCF,
$M_{m/b}$ = Membrane/bending stress intensity magnification factors,
K_m = Misalignment,
In the above expressions, equations for M, f_w, M_m and M_b can be found in BS9710 Appendix M for different types of flawed geometry configurations. For k_{tm}, k_{tb} and k_m, BS9710 part 6.4 and Annex D should be referenced. Eventually, the main result of ECA is the curve of critical crack size or allowable defect size. The curve can be generated by crackwise by selecting flaw height as critical analysis parameter and flaw length as sensitivity analysis parameter.

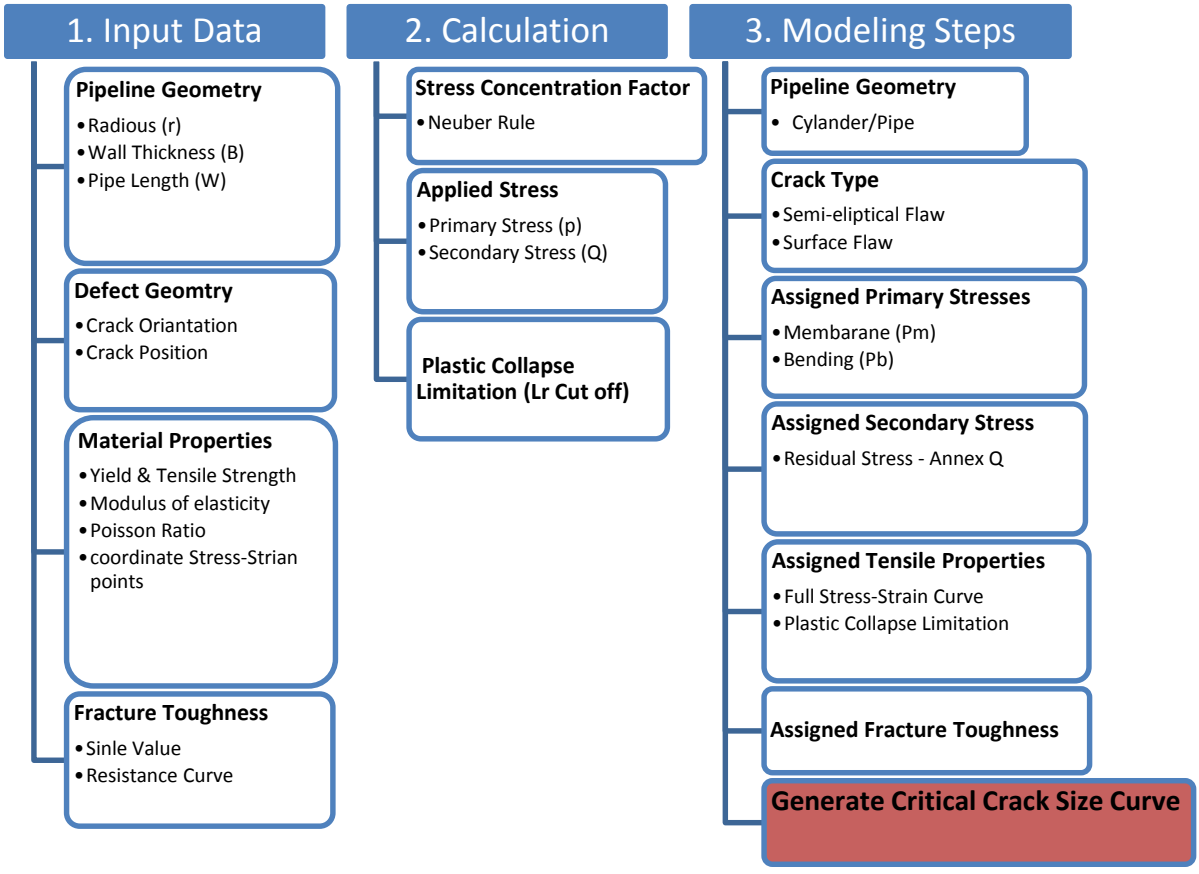

Figure 4 - Crackwise modeling and analysis sequences [16]

3. Results and Discussion

Tolerable defect size curves are presented through Crackwise software according to BS 7910 guideline level 2B and 3B. In level 3B crack ductile tearing is simulated via resistance curves, however in level 2B cracks are assumed to not propagate. According to figure 1, FADs are shown in the form of tolerable crack size curve for axial external and internal surface flaws in compliant with level 2B. Each curve represents specific misalignments that are including 0, 1, and 2 mm misalignment at girth welds. In figure 2, six FADs are presented as in figure 1 but pursuant to level 3B.

It is observed from figure 4 and 5 that by changing in misalignment, the variation in acceptance curve in level 2B for axial internal surface flaws are more than in external flaws. However, the variation between external and internal surface flaws curves are almost identical to each other in level 3B but external flaws still have more evolution. Hence, the influence of girth welds misalignment is more influential for axial internal surface flaws.

(a) (b)

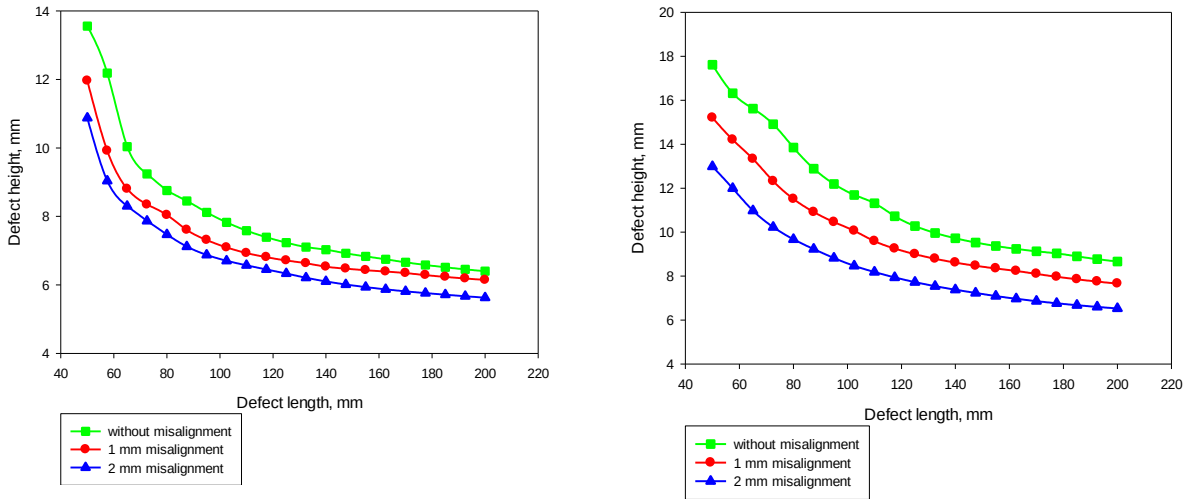

Figure 5- Tolerable defect size curve according to BS 7910- level 2B for axial: (a) Extrnal surface flaw, (b) Internal surface flaw

(a) (b)

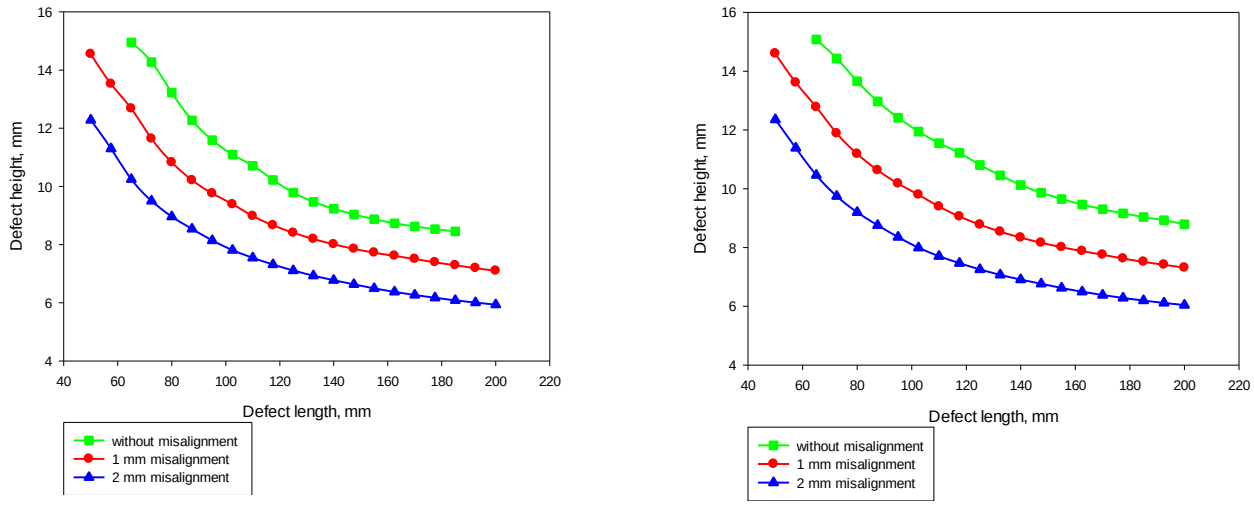

Figure 6-Tolerable defect size curve according to BS 7910- level 3B for axial: (a) External surface flaw, (b) Internal surface flaw

From the figure 6 and 7 the following results can be extracting. The values of defect heights in level 3B for external surface flaws are more than level 2B but whatever the misalignment increases, the amount of flaw heights in level 2B become closer to level 3B. However, for short external surface cracks the difference between flaw heights in level 2B and 3B is more significant than in large cracks. For short internal surface flaws (less than 70 mm), defect heights in level 2B and 3B are adjacent to each other but they are separate with increasing in misalignment amount. However, for large cracks situation is quite the opposite and defect heights get closer with increase in misalignment level.

Internal surface flaws have larger acceptance level for crack heights than external surface flaws especially for short cracks (less than 70 mm). With increasing in misalignment the difference between external and internal flaws heights get reduced. In level 3B external and internal surface flaws have closer results than in level 2B.

Acceptance level for defect heights in circumferential external surface flaws is always larger than axial external flaws. In large cracks, the difference between accepted flaw height between axial and circumferential flaws is greater than in short cracks (less than 70 mm). In the case of internal surface flaws although circumferential cracks still have larger acceptance criteria for defect heights but the difference between axial and circumferential crack heights become greater with increasing in crack length.

(a) (b)

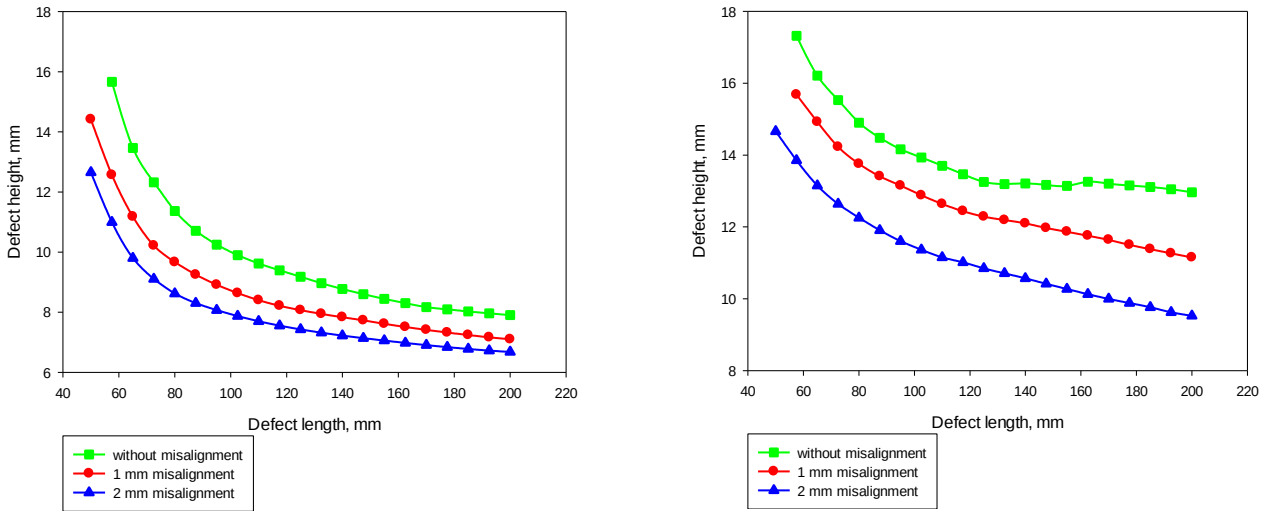

Figure 7-Tolerable defect size curve according to BS 7910- level 2B for circumferential: (a) Extrnal surface flaw, (b) Internal surface flaw

(a) (b)

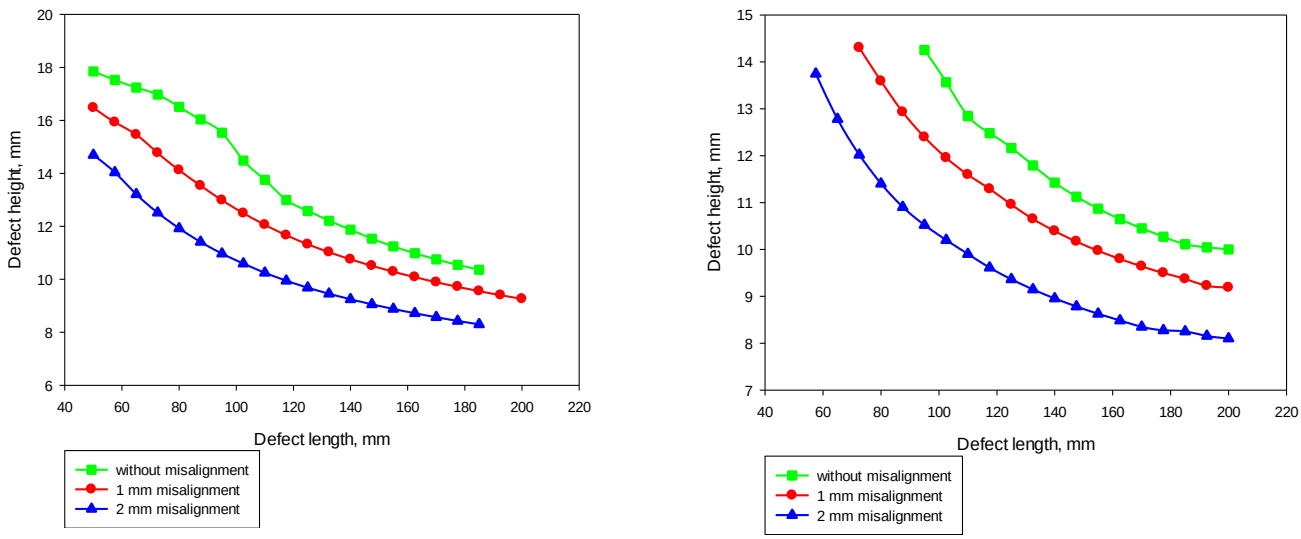

Figure 8- Tolerable defect size curve according to BS 7910- level 3B for circumferential: (a) External surface flaw, (b) Internal surface flaw

4. Summary and conclusions

In the current study, the Engineering Critical Assessment (ECA) of an offshore pipeline with elliptical surface external and internal cracks subjected to different misalignment level under operational loading phase has been analyzed according to BS 7910 level 2B and 3B.Crackwise software is employed to investigate the complex multiple parametric calculations and fracture behavior limit conditions. The influence of the misalignment values, the crack geometries including external, internal, axial, and circumferential flaws on the evolution of FAD in the form of defect acceptance size curves is investigated. The main conclusions and observations are made as follows:

- Influence of misalignment on axial internal flaws is more significant than on axial external flaws, however in level 3B misalignment influence is almost equal on internal and external axial flaws. In the case of circumferential cracks misalignment is more influential for short external cracks (less than 70 mm) but for long cracks it is more significant for internal defects.
- In short external flaws the difference between level 2B and 3B is significant but it becomes smaller for large cracks (larger than 70 mm). for internal cracks the condition is totally vice versa which means that level 2B and 3B for short cracks are almost equal to each other but their difference get larger with increasing in crack length. In both cases increasing in amount of misalignment cause to reduction in crack height acceptance level.
- Internal flaws have always larger values for tolerable defect heights than external surface cracks in both axial and circumferential directions. However the difference between tolerable sizes in level 3B becomes insignificant.
- Circumferential external surface flaws have evermore larger amount of acceptance level in defect heights than axial flaws but with increasing in crack length, acceptance levels for axial and circumferential flaws get closer. However, in the case of internal surface circumferential flaws acceptance levels for crack height is still more than axial flaws but the difference become larger with increasing in crack length.

References

[1] Dake Y, Sridhar I, Zhongmin X, Kumar S B. Fracture capacity of girth welded pipelines with 3D surface cracks subjected to biaxial loading conditions. *International Journal of Pressure Vessels and Piping, vol. 92, no. 11, p. 115-126, 2012.*

[2] Yi D, Idapalapati S, Xiao Z M, Kumar S B. Fracture analysis of girth welded pipeline with 3D embedded subjected to biaxial loading conditions. *Journal of Engineering Fracture Mechanics*; vol. 96: p. 570–587, 2013.

[3] BS 7910, Guide on methods for assessing the acceptability of flaws in metallic structures. BSI, 2013.

[4] Kumar V, German MD, Shih CF. An engineering approach for elastic–plastic fracture analysis. EPRI Report NP-1931. Palo Alto (CA): Electric Power Research Institute; 1981.

[5] Ainsworth R A. The assessment of defects in structures of strain hardening material. Engineering Fracture Mechanics Vol. 19. No. 4. pp. 633-642, 1985.

[6] BS 7910, Guide on methods for assessing the acceptability of flaws in metallic structures. BSI, 2005.

[7] Darcis, Philippe, Diego Santarosa, Naman Recho, and Tom Lassen. "A fracture mechanics approach for the crack growth in welded joints with reference to BS 7910." *15th European Conference on Fracture*, Stockolm 2004.

[8] Pisarski, H., S. Smith, and G. Xu. "Fracture mechanics assessment of flaws in pipeline girth welds." *Welding Research Abroad*, Vol.53, no. 3, 2007.

[9] Permana, I., A Study on Engineering Critical Assessment (ECA) of Subsea Pipeline Girth Welds for Reeling Installation, Master's thesis, University of Stavanger, 2013.

[10] Smith SE., Pisarsk HG., 2010. "A comparison of the API 1104 Appendix A and BS 7910 procedures for the assessment of girth weld flaws," *Journal of Pipeline Engineering*, vol. 9, pp. 120-133.

[11] Larrosa, N. O., and R. A. Ainsworth. "Comparisons of the solutions of common FFS standard procedures to benchmark problems." *International Journal of Pressure Vessels and Piping*, Vol.139, pp. 36-46, 2016

[12] Holtam, C., 2010. Structural integrity assessment of C-Mn pipeline steels exposed to sour environments, PhD dissertation, Loughborough University, 2010.

[13] Wei, L., and Hadley, I., "The effect of bi-axial stress on limit loads of structures containing surface-breaking flaws and its influence on structural integrity assessments." *ASME 2012 Pressure Vessels and Piping Conference*, Toronto, Ontario, Canada, July 15–19, 2012.

[14] Bonora, N., Carlucci, A., Ruggiero, A., and Iannitti, G., "Simplified Approach for Fracture Integrity Assessment of Bimetallic Girth Weld Joint." *ASME 2013 32nd International Conference on Ocean, Offshore and Arctic Engineering*, Nantes, France, June 9–14, 2013.

[15] Wiesnera C S, Maddoxa C S, Xua W, Websterb G A, Burdekinc F M, Andrewsd R M, Harrisona J D. Engineering critical analyses to BS 7910 - the UK guide on methods for assessing the acceptability of flaws in metallic structures. *International Journal of Pressure Vessels and Piping, vol. 77, no. 11, p. 883-893, 2000*.

[16] TWI Software. CRACKWISE 5 help content version 5.0R 27934 Final, 2016.

[17] CSA Z662, "Oil and Gas Pipeline Systems," Canadian Standards Association, 2007.

[18] Wang Y Y, Liu M, Song Y, Horsley D. Tensile strain models for strain-based design of pipelines. Proceedings of the ASME 2012 31st International

Conference on Ocean, Offshore and Arctic Engineering, OMAE2012, Rio de Janeiro, Brazil, July 1-6, 2012.

[19] DNV-RP-F108. Offshore standard – fracture control for pipeline installation methods introducing cyclic plastic strain. Det Norske Veritas, Hovik, Norway; 2006.

[20] Sriskandarajah T, Zhou D. Engineering critical assessment of offshore pipes with partially over matching girth welds during reel lay. *24th International offshore and polar engineering conference* ISOPE. Busan, Korea, June 15-20, 2014.

[21] DNV-OS-F101, Offshore Standard – Submarine pipeline systems. Det Norske Veritas, Hovik, Norway; 2013.

[22] Subsea 7, Technical Guideline for ECA of Reeled Rigid Pipelines, Doc. No. GD-GL-PDCOE- 010, February 2011.

[23] Neuber, H. "Theory of Stress Concentration for Shear Strained Prismatic Bodies with Nonlinear Stress–Strain Law," *Journal of Applied Mechanics*, Vol. 28, No. 4, pp. 544–550, 1961.

[24] Hertele S, Cosham A, Roovers P. Structural integrity of corroded girth welds in vintage steel pipelines. *Journal of Engineering Structures, vol. 124, no. 8, p. 429-441, 2016.*

INTERNATIONAL JOURNAL OF
COASTAL & OFFSHORE ENGINEERING
IJCOE Vol.1/No. 1/Winter 2016 (25-31)

Financial Feasibility Study between Purchasing and Hiring LNG Carrier In Iranian LNG Industry

Meysam Kamalinejad[1], Ali Sheykhbahaee[2]*, Said Mazaheri [3]

[1] *PhD. Candidate on energy systems eng. , K.N.T University; M.Kamalinejad @iranlng.ir*
[2*] *M.E. Student, marine structure eng. , Hormozgan University,A.sheykhbahaee@iranlng.ir*
[3] *Assistant prof.Maritime Tranportation&Tech.Group,TRI,Iran; mazaheri@rahiran.ir*

ARTICLE INFO

Article History:
Received: 24 Sep. 2016
Accepted: 15 Mar. 2016

Keywords:
Economical Sensitivity Analysis, shipping coast, LNG carriers, financial feasibility

ABSTRACT

LNG chain value consists of gas exploration, gas liquefaction, transportation, Re-gasification and finally gas distribution to the end user network. Transportation part of this chain normally consists of 25 to 30% of the total vale and is the most lucrative part of it. As proved Iranian gas reserves is about 29 trillions cubic meter and nearly half of it is South PARS gas field shared between Iran and Qatar ,there is an increasing concern on entering into gas export market in near future.
This enthusiasm enquires a thorough financial study on economical feasibility study on this industry. In this study by emphasizing on key parameters of LNG shipping industry like, technical vessel specification distance between exporting and importing terminals, cost of LNG carriers , boil of ratio of vessels, oil and gas future price prediction vessels heeling portions and most importantly the difference between vessel purchase and hiring daily rate of vessels.
We are to model this industry economically and by doing an economical sensitivity analysis on the model some economical indexes are extracted which are of most benefit for countries decision makers.
Two scenarios of purchasing and renting vessel have been investigated and it is shown than in different financial condition and oil and gas market there are at least minimum internal rate of return of 4 to 18% and at last these finding have been demonstrated in a 3D diagram showing net in come oil price (as an important parameters) and rent daily rate of vessels to show the profitability of this industry to the reader.

1. Introduction

Liquefied Natural Gas, or LNG, is a means of transportation of natural gas. Cryogenically treated natural gas turn into a liquid (LNG), which represents 1/600th of the volume of natural gas, and it is therefore significantly more practical to transport. The natural gas is therefore liquefied at the exporting terminal, transported in special vessels and then re-gasified at the receiving terminal before injected into domestic pipelines and consumed.

Since LNG is no fixed substance which can be traded, is therefore no commodity and demand for LNG is derived from demand for natural gas. It thereby follows that the natural gas market is the underlying market for the LNG market(**Kjersti Hegde**). The traditional LNG market is the foundation of the market, creating security for both sellers and buyers, while the spot market constitutes a possibility for flexibility and speculation. The traditional market will constitute a large portion of the market, as it constitutes a lower risk profile than the spot market. This is also reflected in the forecasted market share of the spot market, so in our study we have based our assumption on traditional LNG market and spot market opportunity is not considered. **(SIMMONS)**
The natural gas market is growing, driven by environmental concerns, the development of combined cycle power generators and embrace of previously "gas poor" countries. Natural gas is the cleanest burning fossil fuel, and is therefore preferred

[DOR: 20.1001.1.25382667.2016.1.0.4.9]

due to new emission policies. The demand if further enhanced by the fact that combined cycle power generators are much more inexpensive than the equivalent coal fired power plant. The embrace of previously gas poor countries has the most direct impact on the future of the LNG market, as the transportation distances are increasing, thereby increasing the volume traded as LNG.

Shipping is an important variable in the LNG value chain Liquefied natural gas (LNG) is expected to play an increasing role in the natural gas industry and global energy markets in the next several years. The combination of higher natural gas prices, lower LNG costs, rising gas imports demand, and the desire of gas producers to monetize their gas reserves is setting the stage for increased global LNG trade.

In this study we asses financial feasibility between purchasing and hiring LNG carriers In Iranian LNG industry which is to be built in Northern shore of Persian Gulf, liquefying natural gas from south pars gas field. **(SIMMONS)**

2. LNG Shipping market

Historically, LNG shipping was covered with long term LNG contracts, typically 20-25 years i.e., basically project financing. Short to medium term markets are dependent on the availability of extra gas which may result in a reduction in liftings under existing contracts, or built-in spare capacity. Availability of spot tonnage today is slowly gaining ground from being virtually non-existent. The year 2008, after a long hiatus, saw 'speculative' ordering of tonnage. Speculative ordering in the next 10 years is expected to give rise to an active spot market, as well as softening of long term shipping rates. Historically, average long term t/c rates have been around US$63-65,000 per day.

LNG shipping plays a critical role in the ongoing expansion of the global LNG industry, especially with the continuing growth of the spot/short-term market and the dynamic expansion of markets and supply sources. The LNG shipping sector is blossoming as it matures: more players, with more ships, mean that more flexible transport contracts can be arranged rather than the traditional long-term commitment of a 'floating pipeline' formed by a fleet that had to be purpose-built for a particular project. ***(*FACTS Global Energy)**

The rapid growth in spot movements is evidence of increased flexibility, and of the attraction for new investors. Although no other shipping sector shows such promise, the whole subject of transporting LNG by sea either through conventional mode or by means of LNG re-gasification vessels which processes the LNG cargo through on board re-gasification plant, delivers natural gas directly from the LNG tanker to the grid was not, until now at such world attention.

For LNG shipping ventures to be viable on long term basis, the ultimate buyer's credibility and the financial strength of all the partners in the supply chain are crucial. In LNG shipping, ships are primarily dedicated to particular projects and these trades between two dedicated terminals almost throughout their life-span. However, spot trading is assuming more significance in the recent years.

By 2009 there were 281 vessels in service with 95 numbers on order. As the global LNG fleet expands and new players enter the market, experience in LNG shipping will be a must to harness opportunities for own requirements, customers and co-ventures.

Table1: Number of delivered and ordered available ships in LNG market

Type	Delivered	On order	Total
Ship	281	95	376
FSRU	1	1	2
FPSO	0	4	4
RV	4	6	10
TOTAL	286	106	392

In the Figure 1 you can see the current and forecasted LNG carrier fleet number till 2020. The forecast of ship demand in standard size units has been derived from a bottom-up estimate of project development over the next 5 years and a top-down appraisal of growth in global consumption and transport capacity requirements .This figure clearly shows the need for more Tankers to be constructed, otherwise the market shall face scarcity in near future and a jump in LNG ships charter rates.

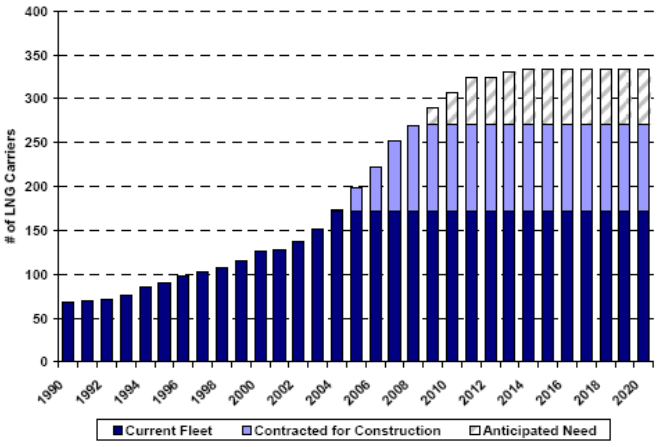

Figure 1: Current and forecasted LNG Carrier Fleet

Anyway spot LNG market's growth is considered to be a lucrative opportunity for LNG Tanker industry and in case of market's shifting from traditional contracts to more liberalized ones, the economy of LNG shipping will be more justified. But to be conservative in our study we haven't considered such opportunities. **(SIMMONS)**

3. Investment costs

According to Andy Flower LNG Associates, there are four main price components to an LNG project: gas

[DOR: 20.1001.1.25382667.2016.1.0.4.9]

production (15-20%), LNG plant (30-45%), LNG shipping (10-30%) and receiving terminal (15-25%).

1.3 LNG cost components

Production cost of LNG has been reduced drastically over the period where it has been traded. Soaring demand for gas initiated the innovation and investments needed to bring down the capital cost. Optimization of design parameters, improved reliability, closed-loop cooling system, exploration of cold-recovery and new heat-exchanger design have all helped reduce the production costs of liquefaction terminals. According to IEA, the average unit investment for a liquefaction plant was $550 per ton per year capacity in 1960s, $350 in 1970s and 1980s, $250 in the late 1990s and slightly below $200 in 2002 and by now it is around $500 per ton per year capacity. **(Saleem Alavi)**

Cost reductions for shipping costs are mainly limited to increasing vessel size. Potentially, an increase in size from 140.000 m3, to 200.000 m3 could decrease shipping costs up to ten percent. Andy Flower estimated that using six 250,000 m3 vessels rather than eleven vessels of 145,000 m3 reduces cost per MMBtu from $0.97 to $0.73.

Building costs for LNG tankers have decreased from about $280 million in the mid1980s to about $155 million in late 2003 and in our study for today's LNG tankers we have assumed $170 million. ***(*FACTS Global Energy)**

2.3 LNG Ship Prices

The prices of LNG ships have varied considerably over time, driven to a large extent by competition for orders amongst the shipyards. The following figure shows the average cost of new ships of between 125,000 m3 and 145,000 m3 capacity, ordered over the last 34 years, and compares it with movements in the cost of very large crude oil carriers (VLCCs). VLCCs are often built in the same construction docks as LNG ships, so the demand for this type of vessel can influence the price of LNG carriers. The prices are the estimated average price of ships ordered in the given year in nominal US dollars. In the late 1980s and early 1990s, the cost of a 135,000 m3 ship (the largest ships in operation at that time) reached over $250 million. Costs fell steadily during the 1990s and by 2003, the cost of a 145,000 m3 ship (typical of the size of ships being ordered at that time) was between $150 and $160 million. However, price has risen again since, partly as a result of the increasing price of steel and other equipment. In 2006, the shipyards are reporting prices of around $220 million for a 155,000 m3 ship**(The World of Energy)**. The prices of the ships over 200,000 m3 ordered for the Qatargas and RasGas projects in Qatar are reported to range from $230 million for the orders for ships around 210,000 m3 placed in 2004 to $290 million for the most recent 270,000 m3 ships. ***(*FACTS Global Energy)**

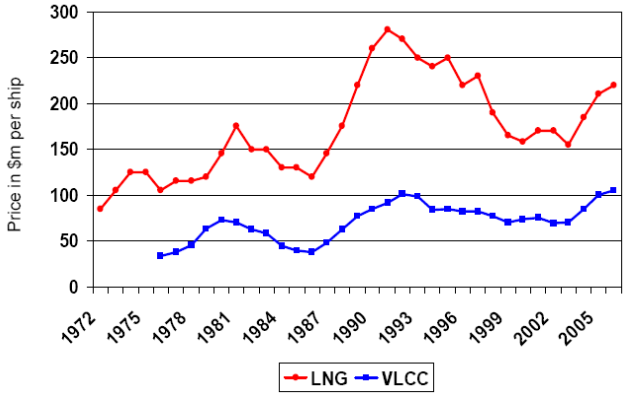

Figure 2: Average LNG Ship (125000 -145000m3) and VLCC Prices In US dollar of the Day

3.3 Operating Costs

There are two main elements in the operating costs of an LNG ship: fixed costs, which are incurred irrespective of the employment of the ship, and voyage costs. The fixed costs include crew, maintenance, administration, and insurance, while the voyage costs include fuel used (bunkers and boil-off), port charges, The fixed costs vary considerably between operators. Crew costs make up a large proportion of the fixed costs and the way in which the ship is crewed. The cost of operating an LNG ship is estimated between $9,000 and $16,000/day. Fuel costs depend on the round voyage distance. Boil-off gas typically provides around 50% of the fuel needs of steam-engine ships, with the remaining fuel being bunker fuel oil. **(Saleem Alavi)**

4.3 LNG Ship Charter Rates

The number of ships in the LNG fleet is a small fraction of the number, for example, of crude oil carriers. Most of the LNG ships in operation are committed to a project or to an LNG buyer. The result is that there are too few charters (short-, medium-, or long-term) arranged for a market index of LNG charter rates to have been developed, The owner of a ship of between 135,000 m3 and 145,000 m3, costing $200 to $220 million is estimated to require a payment of between $45,000/day and $55,000/day to cover the capital cost of the vessel (interest payments, repayment of capital, and return on the equity part of the total capital cost), with the actual rate depending on such factors as interest rates, the share of the investment in the ship covered by loans, and the period over which the cost of the ship is amortized. Adding the $9,000/day to $16,000/day needed to cover fixed operating costs, gives a total charter rate of between $54,000/day and $71,000/day. ***(*FACTS Global Energy)**

[DOR: 20.1001.1.25382667.2016.1.0.4.9]

A number of LNG projects particularly Iran LNG on South Pars are likely to come up in the near future establishing Iran as one of the important LNG exporting countries in the next decade or so. The strategic location of the country being surrounded by other gas-producing countries in the Persian Gulf Region and The Caspian, would require an advanced strategy not only to find a competitive transportation cost but creation of an own fleet of LNG carriers, to guarantee security of exports, independence and the access to the prime markets for the sales of LNG at more interesting pricing as well as a reasonable LNG price for the long term commitments, taking into account the current uncertain situation faced by the world economical crisis.

Considering these points and the above concepts we have investigated a feasibility study on LNG shipping industry.

4. Financial calculation of an LNG Plant owner's entrance into LNG shipping industry

In this part we evaluate if it is profitable and feasible for an LNG plant of 10.5 Million ton LNG per annual to order and purchase LNG tankers or not.

To study this issue we assume that at first the liquefaction plant possesses no ship and during the plant operation it will purchase one tanker each year and as the ship comes into operation the cost of transportation by charter tanker fleet will be reduced annually till the plant owns all its required fleet. By shifting from charter tankers to purchased tanker not only the plant will gain more control over its product and its desired destination and arbitrage opportunity but also there is a good opportunity to get a reasonable net profit. By ordering a new ship the plant will burden an initial capital cost of approximately $170 million and after two years it won't pay for charter.

By obtaining the relative cash flow, which shall be the difference of this expenditure and income obtained from not paying the charter rate we will show the profitability of this cash flow(**Saleem Alavi**).

The variables to be assessed in this study are as below:

1. Initial required capital cost for a tanker is assumed to be $170 million and each year only one ship is ordered
2. Liquefaction Plant capacity which for IRAN LNG is about 10.5 MTPA of LNG
3. Plant and ships lifecycle is assumed t be 25 year
4. The distance between loading and unloading terminals is assumed to be 5000 mile
5. Charter rate of a ship is the source of UNCERTAITY in the study and has a high volatility, so this parameter is assumed to be from 50000 to 130000 dollar per day
6. Ships construction duration is assumed to be 2 year
7. Each ship capacity is around 135000 cubic meter
8. Ship's speed is 19 knot
9. Boil off ratio is 0.15% per day for each ship
10. 2 days is assumed for loading, unloading, berthing and delays
11. Ships and plants overhaul is assumed to be at the same time and once upon 5 year

These parameters have significant effect in LNG transportation industry and any change in one of them will affect decision makers mind and we have been conservative on these assumptions.

The first parameter to calculate financial feasibility for entering into shipping industry for an LNG Plant is to know how many ships are required to transport its product.

Number of required ships is obtained by **Eq. 1**:

$$\text{Number of ships} = \frac{\text{Plant Capacity(Based on Million Ton Per Year)} * \text{Plant Utilization Factor} * \text{Heat capacity of each ton of LNG based on MMBTU}}{\text{Each tanker's Capacity(Cubic Meter)} * \text{Heat capacity of each cubic meter}} \quad \text{Eq. 1}$$

$$\frac{\text{Distance between Ports} * 2}{\text{Ship speed} * 24} + \text{loading, unloading Duration}$$

By considering all previous assumptions at least 13 ships are required to transport the product.

Now we shall calculate cost of transportation based on each MMBTU of the product export. In this calculation we consider boil off loss and heeling loss. As in our calculation we are considering LNG losses during transportation and its consequent expense, we need to have LNG price.

Cost of transportation is obtained by Eq.2:

$$\text{Cost of Transportation per MMBTU} = \frac{\text{Distance between terminal ports} * 2 * \text{Charter Daily Rate}}{\text{Ship Speed} * 24} + \left(1 - \frac{\text{Distance between Ports} * 2}{\text{Ship speed} * 24}\right) * \text{Ship Capacity*Heating Capacity} \quad \text{Eq. 2}$$

LNG price is related to oil price and as we are considering a 25 year cash flow we have to have a

[DOR: 20.1001.1.25382667.2016.1.0.4.9]

prediction for oil price for next 25 year. This prediction is shown in Figure 3.

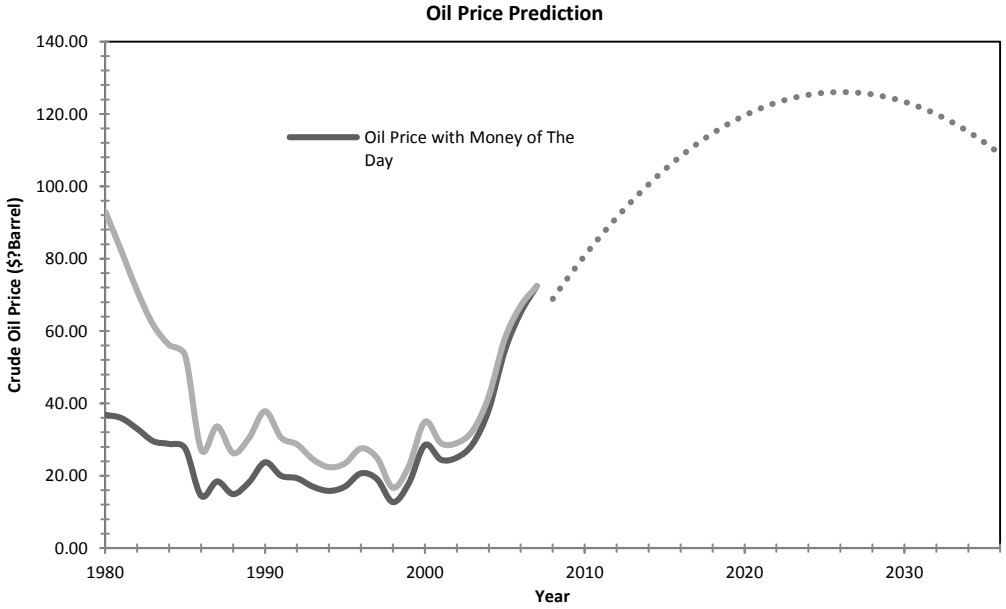

Figure 3: Oil prediction Diagram to obtain LNG Price for boil-off and heeling portion

LNG Price formula is the traditional Japanese formula which is: 0.12 * Oil Price +1.5

The price of boil off and heeling will be obtained by the above formula and is added to the charter rate cost as calculated from above formula and then multiplied by the export volume.

Net difference transportation expense calculation:

- Transportation Cost in case of chartering the fleet:

  In this case the cost of boil-off, heeling and charter rate per MMBTU is calculated and multiplied by product volume
- Transportation Cost in case of chartering and then buying 1 ship annually

  In this case we have to add the cost of each ship annually and after 2 years which is the construction period; we can reduce the cost of relevant charter expense which could be transported by the new ship capacity.

By having these two cash flows, now we can subtract ship purchasing case scenario from chartering scenario. The difference gained from this two expense is the net profit and we can evaluate the Internal Rate of Return of the liquefaction plants entering into shipping industry and owning the tanker fleet.

These calculations are shown in table.2 and table.3 .

Figure 4 shows the cash flow for plant's lifecycle and as it is obvious if charter rate is high enough the plant owners can enter into shipping industry.

Table2: Transportation expenses of a 10.5 MTPA LNG plant using charter to export its product

Daily Charter Rate($/Day)	Ave Expense	2012	2013	2014	2015	2016	2017	2018	2019	2020	2021	2022	2023	2024	2025	2026	2027	2028	2029	2030	2031	2032	2033	2034	2035	2036
50000	188	190	190	190	190	190	175	190	190	190	190	175	190	190	190	190	175	190	190	190	190	175	190	190	190	190
60000	225	228	228	228	228	228	210	228	228	228	228	210	228	228	228	228	210	228	228	228	228	210	228	228	228	228
70000	263	267	267	267	267	267	245	267	267	267	267	245	267	267	267	267	245	267	267	267	267	245	267	267	267	267
80000	300	305	305	305	305	305	280	305	305	305	305	280	305	305	305	305	280	305	305	305	305	280	305	305	305	305
90000	338	343	343	343	343	343	315	343	343	343	343	315	343	343	343	343	315	343	343	343	343	315	343	343	343	343
100000	376	381	381	381	381	381	349	381	381	381	381	349	381	381	381	381	349	381	381	381	381	349	381	381	381	381
110000	413	419	419	419	419	419	384	419	419	419	419	384	419	419	419	419	384	419	419	419	419	384	419	419	419	419
120000	451	457	457	457	457	457	419	457	457	457	457	419	457	457	457	457	419	457	457	457	457	419	457	457	457	457
130000	488	495	495	495	495	495	454	495	495	495	495	454	495	495	495	495	454	495	495	495	495	454	495	495	495	495

Note: All expenses are in Million $, Each five year the plant and tankers go under Overhaul, No inflation is assumed for Charter Daily Rate

[DOR: 20.1001.1.25382667.2016.1.0.4.9]

Table3: Transportation expenses of a 10.5 MTPA LNG plant using charter and then purchasing ships to replace the charter fleet to export its product

Daily Charter Rate($/Day)	IRR	AVE Annual Profit	2012	2013	2014	2015	2016	2017	2018	2019	2020	2021	2022	2023	2024	2025	2026	2027	2028	2029	2030	2031	2032	2033	2034	2035	2036
50000	4%	33	-170	-170	-155	-141	-126	-116	-97	-82	-67	-53	-49	-24	-9	176	190	175	190	190	190	190	175	190	190	190	190
60000	6%	58	-170	-170	-152	-135	-117	-105	-82	-65	-47	-29	-25	6	23	211	228	210	228	228	228	228	210	228	228	228	228
70000	8%	83	-170	-170	-150	-129	-109	-95	-67	-47	-26	-6	-1	35	56	246	267	245	267	267	267	267	245	267	267	267	267
80000	10%	108	-170	-170	-147	-123	-100	-84	-53	-29	-6	17	24	64	88	281	305	280	305	305	305	305	280	305	305	305	305
90000	12%	133	-170	-170	-144	-117	-91	-73	-38	-12	15	41	48	94	120	316	343	315	343	343	343	343	315	343	343	343	343
100000	13%	158	-170	-170	-141	-111	-82	-62	-24	6	35	64	72	123	152	351	381	349	381	381	381	381	349	381	381	381	381
110000	15%	183	-170	-170	-138	-106	-73	-52	-9	23	56	88	96	152	184	387	419	384	419	419	419	419	384	419	419	419	419
120000	16%	208	-170	-170	-135	-100	-65	-41	6	41	76	111	120	181	217	422	457	419	457	457	457	457	419	457	457	457	457
130000	18%	233	-170	-170	-132	-94	-56	-30	20	58	97	135	145	211	249	457	495	454	495	495	495	495	454	495	495	495	495

Note: All expenses are in Million $, Each five year the plant and tankers go under Overhaul, No inflation is assumed for Charter Daily Rate

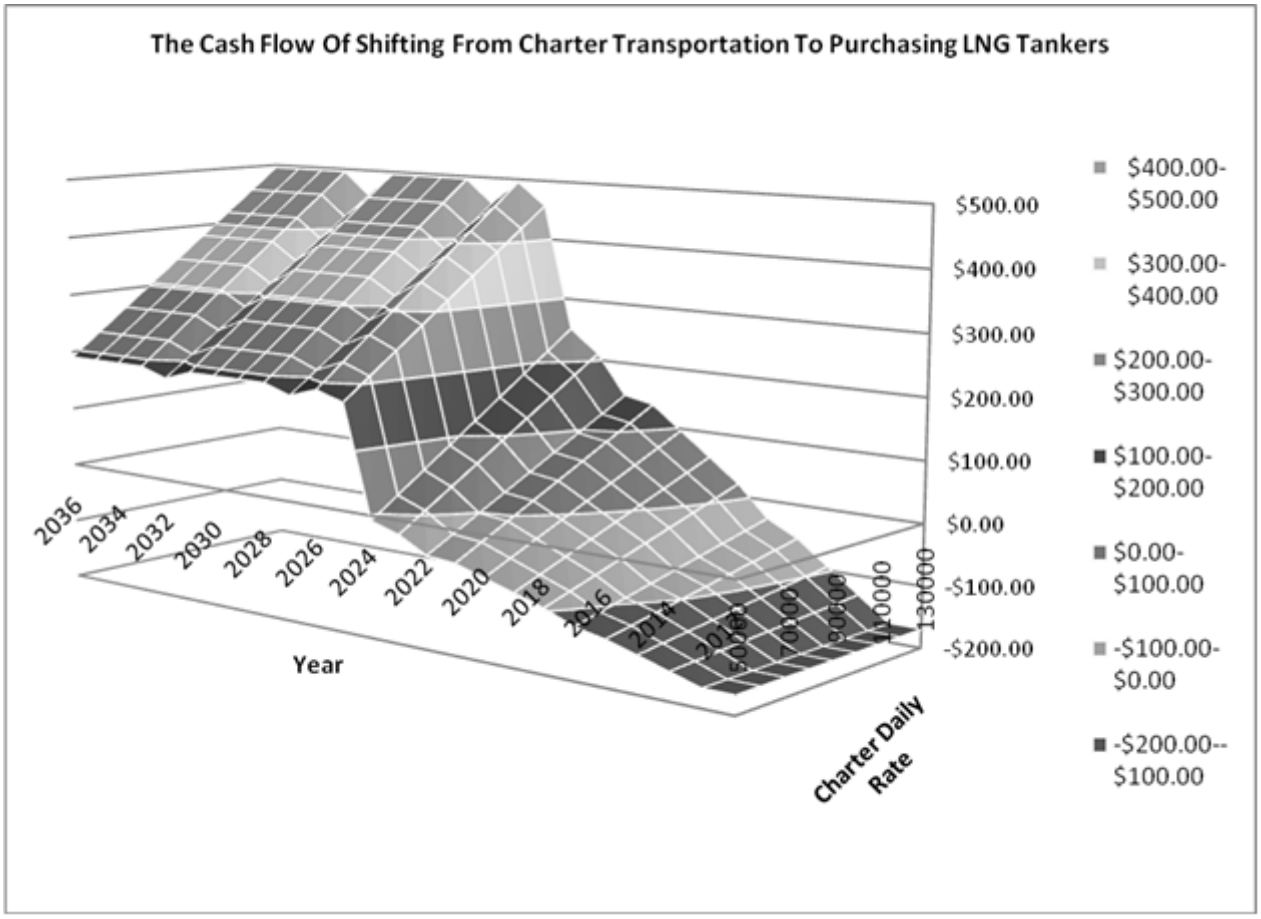

Figure 4: Cash flow sensitivity on charter daily rate between hiring or constructing LNG plant's Private fleet

5. Conclusion

Shipping is an important variable in the LNG value chain Liquefied natural gas (LNG) and is expected to play an increasing role in the natural gas industry and global energy markets in the next several years. LNG shipping plays a critical role in the ongoing expansion of the global LNG industry. A number of LNG projects particularly Iran LNG on South Pars (10.5 MTPA Capacity) are likely to come up in the near future establishing Iran as one of the important LNG exporting countries in the next decade or so. The strategic location of the country being surrounded by other gas-producing countries in the Persian Gulf Region and The Caspian, would require a progressive strategy not only to find a competitive transportation cost fleet but also creation of its own fleet of LNG carriers, to guarantee security of exports, independence and the access to the prime markets for

[DOR: 20.1001.1.25382667.2016.1.0.4.9]

the sales of LNG at more interesting pricing as well as a reasonable LNG price for the long term commitments. In this study by emphasizing on key parameters of LNG shipping industry like, technical vessel specification distance between exporting and importing terminals, cost of LNG carriers , boil of ratio of vessels, oil and gas future price prediction vessels heeling portions and most importantly the difference between vessel purchase and hiring daily rate of vessels. We have modeled this industry economically and by doing an economical sensitivity analysis on the model some economical indexes are extracted which are of most benefit for country's decision makers. Two scenarios of purchasing and renting vessel have been investigated, below figure represents this industry's internal rate of return versus daily charter rate.

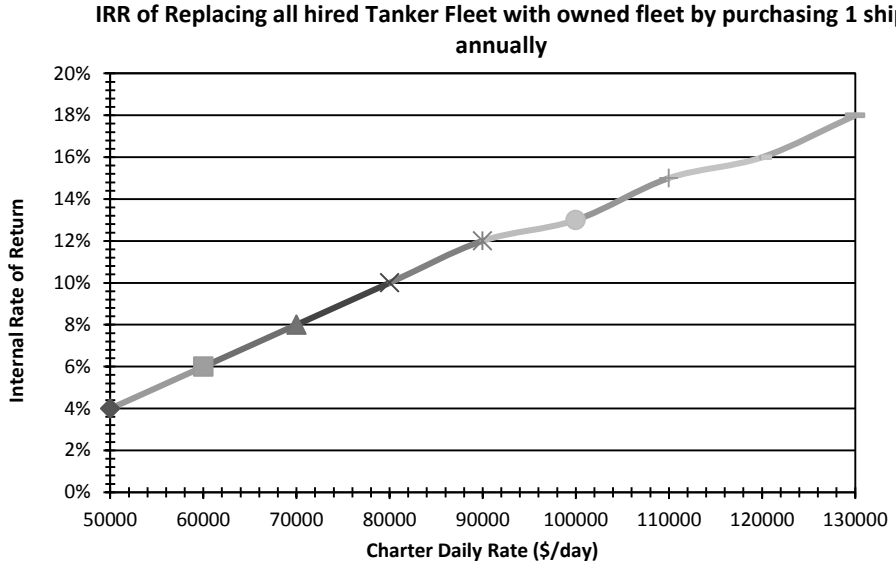

Plant owner's based on their long term policies and favourable independence from charter fleet and the financial indexes shown can decide the entrance into this market.

6. Reference

1. Chapter in a Book

Yoga P. Suprapto (2007). The World of Energy, 26. LNG Ships & Transportation, BADAK LNG, Indonesia

2. Published Thesis

Saleem Alavi(2003-2004) LNG Tanker Market, MSc in Maritime Economics and Logistics, Erasmus University Rotterdam

Kjersti Hegde(2004-2005) The Future of the LNG Spot Market, MSc in Maritime Economics and Logistics, Erasmus University Rotterdam

3. Report

FACTS Global Energy Group of Companies (April 2007) *Evaluating Natural Gas Import Options for the State of Hawaii Prepared for The Hawaii Energy Policy Forum The Hawaii Natural Energy Institute & The Office of Hawaiian Affairs*

Integrated Oil Research, April 7, 2005, *Liquefied Natural Gas*, I N T E R N A T IONAL, SIMMONS & COMPANY

[DOR: 20.1001.1.25382667.2016.1.0.4.9]

INTERNATIONAL JOURNAL OF
COASTAL & OFFSHORE ENGINEERING
IJCOE Vol.1/No. 1/Winter 2016 (33-37)

Concept of Energy Extraction from Sea Waves Using Flapping Foils Operating as Biomimetic System

Ali Zinati[1], Mohammad Javad Ketabdari[2]

[1]*PhD Student, Department of Maritime Engineering, Amirkabir University of Technology, Tehran, Iran; alizinati@aut.ac.ir*
[2]*Associate Professor, Department of Maritime Engineering, Amirkabir University of Technology, Tehran, Iran; ketabdar@aut.ac.ir*

ARTICLE INFO

Article History:
Received: 15 Oct. 2016
Accepted: 15 Mar. 2016

Keywords:
Flapping Foils, Oscillating Hydrofoils, Biomimetic Systems, Energy Extraction

ABSTRACT

Oscillating hydrofoils in presence of waves under the free surface as new systems for energy extraction is a hybrid renewable marine energy sources. In this system energy extraction is associated with oscillating hydrofoils operating as biomimetic systems in harmonic waves and currents in coastal regions using active pitch control. Another way of energy exploiting is used by installation of foils under the hull of the ships. Flapping foils located beneath the hull of the ship are investigated as unsteady thrusters, augmenting ship propulsion in rough seas and offering dynamic stabilization. In this system the foil undergoes a combined oscillatory motion in the presence of waves. For the system in the horizontal arrangement, the vertical heaving motion of the hydrofoil is induced by the motion of the ship in waves. The survey shows that exploiting of energy from sea using these techniques can be proposed for Iranian hybrid ships for their propulsion as secondary source of energy. Particularly North part of Persian Gulf has a proper situation for installation and operation as marine energy device in coastal regions.

1. Introduction

Rising energy bills and intensifying pressure to reduce CO2 emission have caused increasing demand for alternative energy sources for many sectors including marine propulsion. The ocean waves have long been considered as a
substantial source of energy for marine propulsion. However, utilization of wave energy has not been studied extensively because of the complexity of nonlinear oscillatory hydrodynamics. Several experiments have been performed to examine the possibility of utilizing the energy from ocean waves for marine propulsion. In their concept, one or two hydrofoils were fixed to the ship through a spring system, in a manner that the angle of the hydrofoils could be adjusted as the direction of incoming water is changed. In the meantime, the ship and the hydrofoils are heaving and pitching with incoming waves and produce forward thrust on the hydrofoil. The corresponding problem with the moving foil oscillating in an unbounded fluid has been studied for several decades. Swimming of slender fish has been treated by Lighthill [1], and the waving motion of a two-dimensional flexible plate has been calculated. Later, based on the potential flow approach (the perturbation potential is governed by Laplace's equation) [2, 3], a series of researches was performed to optimize the oscillating motion and shape parameters for two-dimensional flat plates. Furthermore, several theories of an oscillating foil have been developed. Bose has developed a time-domain panel method for analysis of an oscillating foil in unsteady motion [2]. Kubota et al. and Kudo et al. [4] developed two dimensional linear and nonlinear theories which can estimate propulsive performance of partly flexible as well as rigid oscillating propulsors. They also showed that an aft-half elastic foil reveals 8% higher efficiency than a rigid foil [4].

2. History and concept

Understanding the interaction of water waves with varying currents in near shore and coastal areas is
important for a variety of engineering applications, including interaction of waves with structures, coastal management and harbor maintenance, as well as design and development of systems for exploitation of marine renewable energy resources. In particular, the effects of inhomogeneous currents on wave transformation in the near shore and coastal environment are significant, since they are responsible for Doppler shifting and additional wave refraction, reflection, and breaking, completely changing the wave energy pattern. In particular, the characteristics of surface waves present significant variation as they

propagate through non-homogeneous ambient currents, in the presence of depth in homogeneities in variable bathymetry regions. Thus, large amplitude waves can be produced when obliquely propagating waves interact with opposing currents. This phenomenon could be further enhanced by inshore effects due to sloping sea beds, and has been reported to be connected with the appearance of giant waves. Extensive analyses concerning the subject of wave-current interaction in the near shore region have been presented by various authors. Recent information can also be found in the corresponding sections of reviewing articles.

Extensive research has been performed in the area of flapping wing aerodynamics and also hydrodynamics. In order to absorb the energy the basic understanding of subject matter, the simple case of rigid hydrofoil / aerofoil in two dimension must be investigate. The vertical structure formed behind these moving foils have a strong link between the motion and the thrust or generated drag. Advanced level of investigation lead to high propulsion efficiency.

Plenty of researches shown that biomimetic systems inspired by hydrobionts not only could produce high thrust but also has a high degree of efficiency. For instance, Bose and Lien [5] estimated that the maximum hydro mechanical efficiency of a whale is about 85%. Furthermore, Triantafyllou, Triantafyllou and Gopalkrishnan [6] and Triantafyllou, Triantafyllou and Grosenbaugh [7] shown that optimal propulsive efficiency occurs at non-dimensional frequencies corresponding to the maximum growth of the jet flow behind the foil.

High efficiency is not the only advantage of a flapping-foil biomimetic system. As Gursul and Ho [8] mentioned, unsteady vortex control creates very high lift coefficients for maneuvering. Additional work on underwater vehicle propulsion and maneuvering has been performed by Bandyopadhyay et al. [9] and Kato [10]. Experimental evidence by Read et al. [11] and Scouveiler et al. [12] also, demonstrates that when flapping foils perform undergoing nonsymmetrical flapping, extraordinary maneuvering capacity occurs. Finally, the three dimensionality of flapping wings and fins has also been studied experimentally by Hart et al. [13], Dickinson et al. [14], and Drucker and Lauder [15].

On the other hand, evolution of air and sea creatures, through million years of natural0selection/optimization, arrived to the flapping wing as their single propulsion system. The main difference between a biomimetic (flapping wing) propulsor and a conventional propeller is that the former absorbs energy by two independent motions, the heaving and the pitching motion, while for the propeller there is only rotational power feeding.

Yamaguchiand [16] Bose extended the work of Kubota et al.. and Kudo et al. [4] to design rigid and aft-half elastic oscillating foils for a large-scale ship. Their results showed that both oscillating foils can give higher propulsive efficiency than an optimal screw propeller, and the elastic foil gives 5–7 % higher propulsive efficiency than the screw propeller. Early hydrodynamics models were restricted to potential flow assumption [3]. But with the advancement of computers, more sophisticated numerical models have been introduced to analyze the performance of an oscillating foil [2]. Pedro et al.. and Guglielmini and Blondeaux [17] have investigated the performance of a low Reynolds number oscillating foil based on a computational fluid dynamics (CFD) approach and promising results have been reported. Other studies (Lai et al. [18], Anderson et al. [19] and Triantafyllou, Triantafyllou and Gopalkrishnan [6]) have addressed the thrust producing capability of an oscillating hydrofoil by experimental work. They have shown that the potential efficiency of the oscillation hydrofoil propulsor can compete with that of a conventional rotating propeller. However, an oscillating hydrofoil has not been considered as a practical replacement because of the mechanical complexity even with the improvement of efficiency up to some extent. Because of that, some of them extended their studies on oscillating foils to consider propulsion by using wave energy as described in the following paragraphs. For the first time in history Wu introduced the theory for extracting energy from surrounding flows by a two-dimensional hydrofoil oscillating through gravity waves in water. According to his theory, it has been found that the energy extraction is impossible if the flow is uniform and only feasible when the primary flow contains a wave component which has vertical velocity normal to the mean free stream and the wing span. Finally, he was able to obtain the best mode of heave and pitching for extraction of wave energy by passive type wave devouring propulsor. Later, Isshiki [20] employed Wu's theory of an oscillating hydrofoil and extended it by introducing a free surface effect for investigating the possibility of wave devouring propulsion by a passive type oscillating hydrofoil. Further, not only theoretically, but also experimentally, Isshiki and Murakami [21] studied the basic concept of passive type wave devouring capability of an oscillating hydrofoil. In addition, to illustrate the unsteady foil motions and wave devouring capabilities, Grue et al. [22] developed a theory for a two-dimensional flat plate near the free surface using a frequency-domain integral equation approach. The theory in both head and following waves was in good agreement with the experiment conducted by Isshiki and Murakami; however, with lower wave numbers there were systematic discrepancies between the theory and the

experimental results as nonlinear effects and free surface effects were not fully accounted for in the theory. Despite these inviting results by several independent studies, a significant commercial success is yet to be seen. The drawbacks of the concept have added resistance in calm seas as well as mechanical complexity. Although the oscillating foil propulsor is mechanically complex, if the gain by recovering the wave energy is considerable, it may be more attractive than the conventional screw propeller. In the present study, therefore, we propose a new concept of wave energy recovering through a powered oscillating foil propulsor, which is designed to replace the conventional screw propeller "Figure 1". The objectives are to develop a numerical model which can predict the oscillating foil performance in a wave field and to elucidate the physical mechanisms.

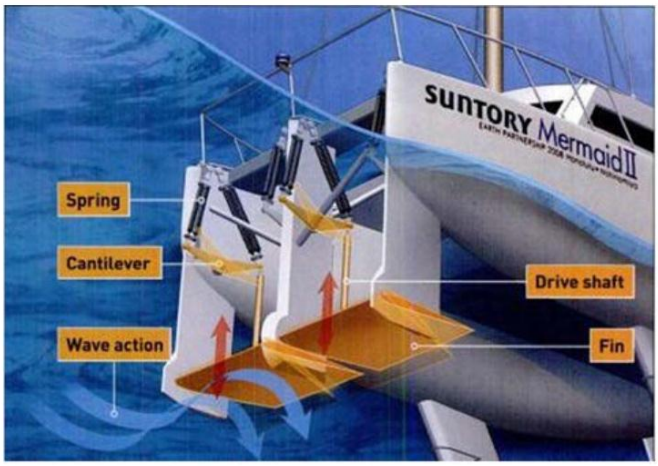

Figure 1: The Suntory Mermaid II which sailed from Hawaii to Japan in 2008 (Popular Science, 2008) [23]

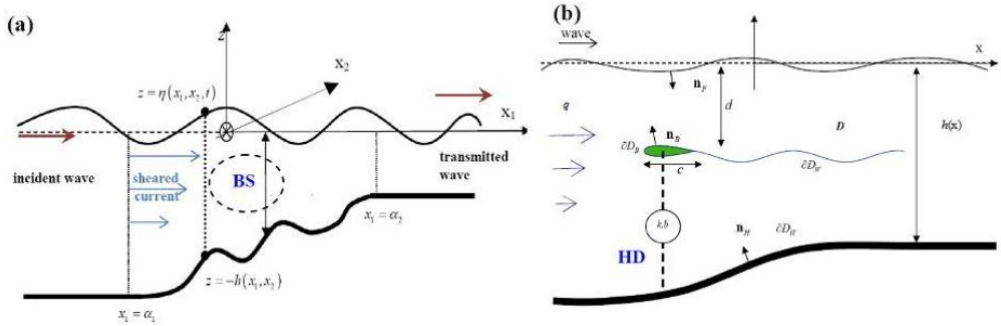

Figure 2: a) Interaction of waves with vertically sheared currents over variable seabed topography. b) Flapping hydrofoil biomimetic system(BS) operating as energy device in waves and sheared currents.

3. Motion of flapping foils

The flapping motion of large aspect ratio wings with two-dimensional foils in harmonic pith and heave motion has been studied intensively in response to the demand for faster and simpler simulation. The NACA0012 hydrofoil is the benchmark model. Others have used conformal mapping Joukowski or elliptical foils. Moreover, more complex unsteady motions are studied, starting with simple forward and heaving motion or forward and pitching motion and finally flapping motion. The latter consists of forward, heaving and pitching motion

4. Pure heave motion

A Combination of reduced frequency and normalized heave amplitude has been found to be a good parameter to predict the drag-thrust wake pattern. Heave amplitude is normally defined divide by chord length. Lai and Platzer find that a drag-producing wake behind a pure heaving NACA0012 foils changes to a thrust-producing jet as soon as ratio of maximum heave velocity to free stream speed or the non-dimensional heave velocity "Figure 4(a)".

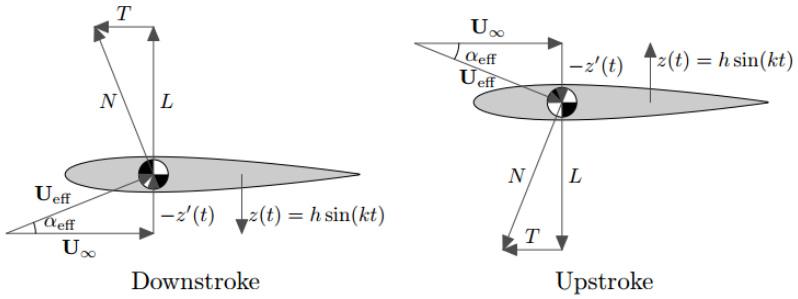

Figure 3: Explanation of thrust generation by pure heave motion

5. Pure pitch motion

pure pith motion is the only case where thrust is generated when there is no forward velocity. A strong influence on the corresponding wake patterns of the amplitude, frequency and the shape of oscillation waveform was also identified. The reduced frequency for vortex roll-up is found to decrease as the oscillation amplitude increases "Figures 3 and 4(b)".

6. Combined heave and pitch

The case of combined heave and pitch is often found in flapping wing propulsion in nature. The flapping motion to be a better strategy than the pure heave and pitching alone as it is more efficient and higher thrust can be generated [24]. The complexity of coupling the two motions, heaving and pitching, means that two more parameters are needed to add to the current set. They are the additional amplitude and phase angle between heave and pitch "Figure 4(c)".

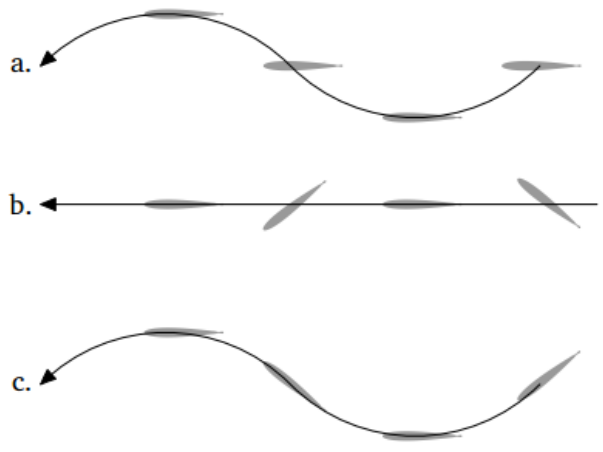

Figure4:a) Pure heaving and forward motion b) Pure pitching and forward motion c) Combined heaving and pitching and forward motion

7. Results and Discussion

The current flow is assumed to vary very slowly as it is in the case of tidal and low frequency environmental flows, so that it may be considered steady at the scale of wave evolution. The current is characterized by a vertical variation will be stronger that the horizontal one, so that the vorticity associated with the background flow is essentially horizontal like the current itself. The current flow velocity is small and thus, the associated mean free-surface elevation (set-down) is also small. The wave flow perturbing the background current flow, is generated by an incident wave system coming from the far up-wave region. One of the application of flapping hydrofoil biomimetic system is extraction of energy from sea in harmonic waves and current in coastal regions using pitch control [25]. Interaction of waves with vertically sheared currents over variable seabed topography. One of the most important factor is geometry of coastal regions because of interaction of wave and seabed. This specification of geometry of sea is related of north part of Persian gulf where along of coast depth of water has a proper situation "Figure 2".

8. Conclusions

Oscillating hydrofoils in waves and currents are investigated as novel biomimetic systems for extraction and exploitation of this kind of marine renewable energy. The effects of the wavy free surface through the satisfaction of the corresponding boundary conditions, as well as the velocity component due to waves and vertically sheared currents on the formation of the incident flow were investigated. After validation, it could be found that it is useful for the design and optimum control of such biomimetic systems operating in the near shore/coastal region and extracting energy from waves and ambient currents.

References

[1]Lighthill MJ., Note on the swimming of slender fish. J. Fluid Mech. Vol. 9, pp. 305–17, 1960.

[2] Bose, N., ‘‘A time-domain panel method for analysis of foils in unsteady motion as oscillating propulsors’’, 11th Australasian Fluid Mechanics

Conference University of Tasmania, Australia 14-18 Dec. 1992.

[3] Ghassemi, H., and Kohansal, A.R., ‘‘Boundary element method applied to the lifting bodies near the surface’’, Journal of marine engineering, Vol.5, No.10, 2010.

[4] Kubota, A., and Kudo, T. and Kato, H. and Yamaguchi, H. ‘‘Study on propulsion by partially elastic foil (1nd, 2nd report)’’ J Soc Nav Arch Japan, Vol. 156, pp. 85–105, 1984.

[5] Bose N. and Lien J. ‘‘Propulsion of a fin whale (Balaenoptera physalus): why the fin whale is a fast swimmer’’, Proceedings of the Royal Society of London B, Vol. 237, pp. 175-200., 1989.

[6] Triantafyllou M.S., Triantafyllou G.S. and Gopalkrishnan R. ‘‘Wake mechanics for thrust generation in oscillating foils’’, Phys. Fluids, A Vol. 3, No. 12,1991.

[7] Triantafyllou M.S., Triantafyllou G.S. and nGrosenbaugh M.A. ‘‘Optimal thrust development in oscillating foils with application to fish propulsion’’, Journal of Fluids and Structures, Vol. 7, pp. 205-224, 1993.

[8] Gursul I. and Ho C.M. ‘‘High aerodynamic loads on an hydrofoil submerged in an unsteady stream’’, AIAA Journal, Vol. 30, pp. 1117-1119, 1992.

[9] Bandyopadhyay P., Castano, J., Rice, J., Phillips, R., Nedderman, W. and Macy, W.,‘‘Lowspeed maneuvering hydrodynamics of fish and small underwater vehicles’’, Journal of Fluids Engineering, Vol. 119, pp. 136–144, 1997.

[10] Kato N., ‘‘Locomotion by mechanical pectoral fins, Journal of Marine Science and Technology’’, Vol. 3, pp. 113–121, 1998.

[11] Read D.A.,Hover F.S. and Triantafyllou M.S., ‘‘Forces on oscillating foils for propulsion and maneuvering’’. J. Fluids Structures Vol. 17, pp. 163-183, 2003.

[12] Schouveiler L., Hover F.S. and Triantafyllou M.S., ‘‘Performance of flapping foil propulsion’’. J.Fluids Structures Vol. 20, pp. 949-959, 2005.

[13] Hart D., Acosta A., Leonard A., ‘‘Observations of cavitations and wake structure of unsteady tip vortex flows, In Proceedings of the International STG Symposium on Propulsors Cavitations’’, Hamburg, Germany, pp. 121-127., 1992.

[14] Dickinson M.H., Lehmann F.O., Sane S.,‘‘Wing rotation and the aerodynamic basis ofinsect flight’’, Science, Vol. 284, pp. 1954-1960, 1999.

[15] Drucker E.G. and Lauder G.V.,‘‘Locomotor forces on a swimming fish: three-dimensional wake dynamics quantified using digital particle image velocimetry’’, Journal of Experimental Biology, Vol. 202, pp. 2393–2412., 1999.

[16] De Silva L.W.A. and Yamaguchi H., ‘‘Numerical study on active wave devouring propulsion ’’,Journal Marine Science & Technology Vol. 17, pp. 261-275, 2012.

[17] Guglielmimini L. and Blondeaux P.,‘‘ Propulsive efficiency of oscillating foils. European journal of mechanics’’, B/Fluids,Vol. 23, pp.255-278, 2004.

[18] Lai J.C.S. and Platzer M.F.,‘‘Jet characteristics of a plunging hydrofoil’’, AIAA Journal, Vol. 37,pp. 1529-1537,1999.

[19] Anderson J.M., Streitlien K., Barrett D.S. and Triantafyllou M.S.,‘‘Oscillating foils of highpropulsive efficiency’’. J. Fluids Mech. Vol. 360, pp. 41-72,1998.

[20] Isshiki H.,‘‘A theory of wave devouring propulsion’’. J Soc. Nav. Archit. Japan Vol. 151, pp. 54–64, 1982.

[21] Isshiki, H. and Murakami, M.,‘‘A theory of wave devouring propulsion’’, J Soc Nav Arch Japan, Vol. 156, pp. 102–114, 1984.

[22] Grue J., Mo A., Palm E., , ‘‘Propulsion of a foil moving in water waves‘‘, J. Fluid Mech., 186, 393-417, 1988.

[23] Geoghegan, J., "Boat moved only by waves, Sails to a seafaring first", The New York Times, July 8, 2008.

[24] Kostas, A., and Belibassakis, K.A., ‘‘Marine propulsion in wave by flapping-foil systems’’, 8th GRACM International Congress on Computational Mechanics Volos, 12 – 15 July 2015

[25] Belibassakis, K.A., Filippas, E.S., and Gerostathis, Th.P., Biomimetic systems operating as marine energy devices in waves and sheared currents’’, 11th HSTAM International Congress on Mechanics Athens, 27–30 May, 2016, Greece.

Volume & Issue:

Volume 1, Issue 1, April 2016

Number of Articles: 5

Content